



# Effects of curing cycles on developing strength and microstructure of goethite-rich aluminosilicate (corroded laterite) based geopolymer composites

Joelle Nadia Nouping Fekoua, Cyriaque Rodrigue Kaze, Linda Lekuna Duna, Ameni Gharzouni, Ibrahim Mbouombuo Ndassa, Elie Kamseu, Sylvie Rossignol, Cristina Leonelli

## ► To cite this version:

Joelle Nadia Nouping Fekoua, Cyriaque Rodrigue Kaze, Linda Lekuna Duna, Ameni Gharzouni, Ibrahim Mbouombuo Ndassa, et al.. Effects of curing cycles on developing strength and microstructure of goethite-rich aluminosilicate (corroded laterite) based geopolymer composites. Materials Chemistry and Physics, 2021, 270, pp.124864. 10.1016/j.matchemphys.2021.124864 . hal-03283727

**HAL Id: hal-03283727**

**<https://unilim.hal.science/hal-03283727>**

Submitted on 2 Aug 2023

**HAL** is a multi-disciplinary open access archive for the deposit and dissemination of scientific research documents, whether they are published or not. The documents may come from teaching and research institutions in France or abroad, or from public or private research centers.

L'archive ouverte pluridisciplinaire **HAL**, est destinée au dépôt et à la diffusion de documents scientifiques de niveau recherche, publiés ou non, émanant des établissements d'enseignement et de recherche français ou étrangers, des laboratoires publics ou privés.



Distributed under a Creative Commons Attribution - NonCommercial 4.0 International License

# Effects of curing cycles on developing strength and microstructure of goethite-rich aluminosilicate (corroded laterite) based geopolymer composites

Joelle Nadia Nouping Fekoua<sup>1,2,3,4\*</sup>, Cyriaque Rodrigue Kaze<sup>1,2\*</sup>, Linda Lekuna Duna<sup>2</sup>, Armeni Ghazouni<sup>3</sup>, Ibrahim Mboumbuo Ndassa<sup>4</sup>, Elie Kamseu<sup>2,5\*\*</sup>, Sylvie Rossignol<sup>3</sup>, Cristina Leonelli<sup>5</sup>

<sup>1</sup>Laboratory of Applied Inorganic Chemistry, Faculty of Science, University of Yaoundé I, P.O. Box 812, Yaoundé, Cameroon.

<sup>2</sup>Laboratory of Materials, Local Materials Promotion Authority, MINRESI/MIPROMALO, Yaoundé, Cameroon Po. Box, 2396 Yaoundé-Cameroon Tel/Fax : +237 222 22 37 20.

<sup>3</sup>UMR CNRS 7315, CEC, Institut de Recherche sur les céramiques (IRCER), Université de Limoges, 12 Rue Atlantis, Limoges, France.

<sup>4</sup>Computational Chemistry Laboratory, High Teacher Training College, University of Yaoundé I, P.O. Box, 47, Yaoundé, Cameroon.

<sup>5</sup>Department of Engineering “Enzo Ferrari”, University of Modena and Reggio Emilia, ViaP. Vicarelli 10, 41125, Modena, Italy.

\*Corresponding authors: noupiming@yahoo.fr (J.N.N Feukoua); kazerodrigue@gmail.com (R.C Kaze)

\*\*Corresponding author. Laboratory of Materials, Local Materials Promotion Authority, MINRESI/MIPROMALO, P.O. Box 2396, Yaounde, Cameroon.

kamseuelie2001@yahoo.fr (E. Kamseu)

33

34       **Effects of curing cycles on developing strength and microstructure of**  
35       **goethite-rich aluminosilicate (corroded laterite) based geopolymer**  
36       **composites**

37

38   Abstract:

39       The present work carried out the influence of curing cycles on the performance of  
40   laterite-based geopolymer composites. To do so, the end products were obtained by altering  
41   laterite with 15, 20, and 25 wt.% of rice husk ash (RHA). Alkaline solution in a constant  
42   solid/liquid ratio of 0.35 was added together with fine and coarse aggregates (representing  
43   equal and double weight of laterite, respectively). The different obtained matrices were  
44   treated in the following three curing cycles before characterization: room temperature curing  
45   (RTC), oven curing at 80 °C (OTC) and controlled humidity steam curing at 80 °C (STC).  
46   The mechanical tests carried out at 28 days give the following maximum values for each  
47   curing mode: 16.40, 28.82 and 56.41 MPa for RTC, OTC, and STC modes respectively. This  
48   means that when the samples, submitted in a moisture-controlled environment, the end  
49   products are more stable, less porous and resistant. Regarding the physical properties, the  
50   results show that the maximum value of open porosity is 11.62 % corresponding to a matrix  
51   that was cured at room temperature without rice husk ash added, while the minimum value of  
52   7% corresponds to a matrix that was cured under controlled humidity and containing 20% rice  
53   husk ash. The optimum and minimum absorption values are 2.70 and 4.60% respectively for  
54   the OTC and RTC curing modes. As for bulk densities, the optimum value is 2.64 g.cm<sup>-3</sup> for  
55   the matrix having 15% rice husk ash and the minimum value is 2.33 g.cm<sup>-3</sup> for a matrix  
56   having 20% rice husk ash, for OTC and STC curing modes respectively. The appropriate  
57   curing type for laterite-based geopolymer is when the humidity is controlled.

58

59   Keywords: laterite, curing cycles, quarry sand dust, rice husk ash, mechanical properties,  
60   microstructure, porosity

61

62

63

## 1. Introduction

Geopolymers are known as alternate binders and composites are obtained from a mixture between an aluminosilicate material powder and an alkaline solution (NaOH, Na<sub>2</sub>SiO<sub>3</sub> etc.) or acid solution (H<sub>3</sub>PO<sub>4</sub>) at relatively low temperature ( $\leq 100$  °C) [1-4]. Its structure consists of repeating units of the chemical Si-O-Al, Si-O-Al-Fe and Si-O-Al-P bonds depending on the characteristics of the solid precursors, conditions synthesis and reagents type used for their production [5-9]. The current aluminosilicate materials largely used in the synthesis of geopolymers are metakaolin obtained by dehydroxylation of kaolin and halloysite clays heated in the range of 500-750 °C [2, 3, 10-13], fly ashes [14-16] and volcanic ashes [17, 18] etc. Recently laterites have gained more attention and were used as potential solid precursors for the synthesis of geopolymer binders and composites with the final properties correlating with the synthesis conditions, curing process and their chemical and mineralogical composition [1-3, 7, 19-26]. Most of the relevant above-mentioned published works have focussed on calcined laterites between 500 and 700°C and few conducted on raw laterites. From the literature, laterites are reddish and yellowish soils formed in tropical and sub-tropical regions worldwide. They are formed through induration or laterization phenomenon in which the kaolinite is corroded by iron minerals such as goethite, hematite, ilmenite, etc. accompanied by the substitution of Al<sup>3+</sup> in kaolinite octahedra site by Fe<sup>2+</sup> or Fe<sup>3+</sup> atoms release by iron minerals [6, 7, 19, 25, 27]. This structural disorder that occurred in corroded laterites affects their crystallinity and justified why this material does not need highly thermal energy activation for their dehydroxylation compared to standard kaolin clay. Kaze et al. [19, 25] and Kamseu et al. [7], using raw corroded laterites without calcination in the presence of amorphous silica from rice husk ash (15, 20, and 25 wt% by weight) in the laterite based geopolymer composites synthesis to make low-cost, eco-friendly and environmentally materials for the so-called synthesis under controlled relative humidity and curing cycles. These authors also showed that the combined actions of reactive silica and fine quartz sand necessary to polymerize free Al-, Si- and Fe- oligomer species within the iron-rich laterite based geopolymer composite matrices by forming Na-poly-ferro-sialate (-Si-O-Al-Fe-) and Na-poly-sialate(-Si-O-Al) binder phases required for the better connectivity or cohesion between different particles or components in the matrix. Kamseu et al. [7] claimed that the densification of laterite based geopolymer composite matrix from corroded laterite altered by rice husk ash at different dosages, oven-cured at 90°C is related to the formation of strong Fe-O-Si bonds leading to new formed phases like hinsingerite. The dense and compact

geopolymer matrix exhibited the interconnected pores which found potential application in filtration or encapsulation of heavy metals. Whereas, Kaze et al. [25] claimed that the flexural strength achieved in the range of 6-40 MPa was due to the formation of ferrisilicate that improved the mechanical properties making this new cementitious material as potential building materials.

To minimize the energy and calcination temperature of clayey materials, several authors altered metakaolin by fine semi-crystalline materials such as feldspar, granite, sand [7, 28, 29] for the synthesis of geopolymer composites. The resulting products developed high flexural strength and well-densified matrix leading to the increase in amorphous geopolymer binder from dissolution of fine aggregates in alkaline solution. Previously, Tchadjie et al. [30] obtained 41 MPa from alkali-activated waste granite by alkaline fusion method. It is well known that the need of aggregates (basalt, granite, gneiss, etc.) in concretes production increased with infrastructures development especially in low-income as well as developed countries. However, the production of aggregates scraps for the buildings construction release sawdust which can cause silicosis when inhaled by humans or contaminates the soils [31]. On the other hand, there is no efficient use (civil engineering application) of these aggregates' sawdust released from quarry factories. Therefore, it is urgent to valorize these wastes to limit their environmental impact. For environmental protection, this work firstly aimed to mix raw iron-rich laterite/quarry sand dust as solid precursor altering by, 30, 40, and 50 wt% of rice husk ash (RHA) for the production of low-cost materials for buildings purpose by applying geopolymerization process under controlled humidity and curing cycle. In addition, the effects of alkaline solution and curing cycles (room curing temperature (RTC), oven curing temperature (OTC), and steam curing temperature (STC) on microstructural, physicochemical and mechanical properties of laterite-based geopolymer composites samples were investigated. When consider the room temperature curing, the humidity is easily controlled but the temperature seems not to be enough for the efficient reactivity of iron. During oven curing, the earlier evaporation of water is responsible for the development of interconnected pores with limitation of the reactivity of iron. It is expected that, the control of humidity in the range of temperature that favours the reactivity of iron, will improve the densification of mechanical strength. The binder phases in different hardened products were assessed using XRD, FTIR, DTA/TG and ESEM/EDS. The mechanical and physical properties were obtained by means of flexural strength, water absorption, bulk density and apparent porosity.

The obtained results are interpreted by correlating the curing cycle types, microstructure and mechanical strength.

## 2. Materials and experimental Technique

### 2.1 Materials and alkaline solution

The solid precursors, i.e., laterite and rice husk ash, were crushed and sieved down 63  $\mu\text{m}$ . Quarry sand dust was collected and sieved down 63  $\mu\text{m}$ . The none passing particles of quarry sand having size between 350  $\mu\text{m}$  and 5.00 mm were used as aggregate. The laterite and quarry sand were collected respectively at Emana and Akak in Yaoundé town, Centre Region Cameroon. Whereas rice husk ash was obtained from the rice factory located in Ndop, North West Region, Cameroon.

Alkaline solution was obtained by a mixture of a commercial sodium silicate solution (%Na<sub>2</sub>O: 14.37; %SiO<sub>2</sub>: 29.54 and %H<sub>2</sub>O: 56.09, supplied by Prolabo Chemicals, France) with an 8 mol/L of sodium hydroxide solution (obtained by diluting the pellets of commercial NaOH with 99 % of purity, supplied by Prolabo Chemicals, France). The weight ratio of sodium silicate to NaOH solution was equal to 2. The prepared alkaline solution was kept in the laboratory for 24 h before used in order to depolymerize the long chain of silica species.

### 2.2 Elaboration of geopolymer composite samples: GL<sub>1-y-z</sub>R<sub>y</sub>F<sub>z</sub>S

The laterite-based geopolymer composites were labelled GL<sub>1-y-z</sub>R<sub>y</sub>F<sub>z</sub>S, where y represents the weight percentage (wt.%) of rice husk ash (RHA) in total powders and 1-y-z the weight percentage (wt.%) of laterite. z stands for the fixed percentage (50 wt.% of total powder) of fine aggregate labelled F. The laterite-based-geopolymer composites were produced by firstly mixing the solid precursors in a Hobert mixer until a homogeneous powder is obtained. The alkaline solution was introduced in a liquid/solid ratio of 0.35 that allowed acceptable workability and mixing for 5 min. Then the coarse quarry sand was added in powder (laterite + rice husk ash + fine aggregates)/coarse aggregates ratio of 1/2 and the mix was once more mixed for another 5min. The resulting geopolymer composite pastes from each formulation poured into parallelepipedal moulds with dimensions of 80 x 20 x 20 mm. The details for the mix design and synthesis of laterite based geopolymer composites are given in Table 1. The obtained samples were subjected to three different types of curing: Room temperature curing (RTC), Oven temperature curing (OTC) at 80°C, and Steam temperature curing (STC) (under controlled relative humidity). For the room temperature curing, the samples were placed at room temperature after demoulding until mechanical test performed. In case of oven curing,

48 h keeping at room temperature after moulding, the samples were placed in the oven and removed 24 hours later before being removed from the moulds. Finally, for hydrothermal curing, 48 h after moulding, the samples were placed in a steam curing chamber at 80 °C with controlled humidity (65 %) for about 7 h. All the laterite-based geopolymer composite samples obtained from different curing regimes were subjected to flexural strength measurements, porosity, water absorption, bulk density after 28 days.

Table 1: Geopolymer composite compositions

Mixture ID	L (g) laterite	RHA (g) Rice husk ash	Fine Quarry Sand(g)	Coarse Aggregates (g)	Alkaline solution (g)
GL <sub>0.5</sub> R <sub>0</sub> F <sub>0.5</sub> S	50	0	50	100	35
GL <sub>0.35</sub> R <sub>0.15</sub> F <sub>0.5</sub> S	35	15	50	100	35
GL <sub>0.3</sub> R <sub>0.2</sub> F <sub>0.5</sub> S	30	20	50	100	35
GL <sub>0.25</sub> R <sub>0.25</sub> F <sub>0.5</sub> S	25	25	50	100	35

## 2.3 Characterization methods

### 2.3.1 Chemical and thermal characterization

#### 2.3.1.1 X-ray Fluorescence

The X-ray fluorescence is an analysis that permits to find out the chemical composition of the sample. The chemical compositions of raw materials (laterite, rice husk ash, quarry sand) were determined using a Zetium PANATICAL apparatus at a power of 1 KW. Before carried out the analysis, each sample powder was mixed with lithium borate salt and vitrified within a Pt crucible at 1600 °C.

#### 2.3.1.1 Thermal and gravimetry analysis

Differential Thermal Analysis (DTA) coupled with Thermogravimetry analysis (TG) is an analytical technique that allows changes in the physicochemical states of compounds subjected to temperature variations. These changes are manifested by exothermic or endothermic phenomena. DTA measures the evolution of the temperature difference between the sample and an inert control body, thus indicating the different thermal phenomena. The coupling with the TG, which measures mass losses as a function of temperature, makes it possible to determine the contribution of the different peaks. The thermal analysis was measured using the "SDT Q600 from TA instruments". The material analyses were carried out under the following conditions: between 30 and 900 °C at a speed of 5°C/min for 15min; about 30 mg was introduced into a platinum crucible under air flushing. The sample and the reference were placed in two identical platinum crucibles.

### 2.3.1.3 X-ray Diffraction

The X-ray diffraction is a structural analysis based on the interactions between X-ray and matter. It is consisting of sending a beam of X-ray of wavelength  $\lambda$  on a sample. When the wavelength is the same order of that of magnitude at the inter-reticular distance ( $d$ ), the beam is diffracted by the crystal plane according to Bragg's equation:  $2d_{hkl}\sin\theta = n\lambda$ . Scattered rays interfere and lead to the phenomenon. The pieces collected from mechanical testing of each product formed (laterite-based geopolymer composites) were ground and sieved through 63  $\mu\text{m}$ . The obtained powders and the raw materials were subjected to XRD analysis to identify the mineral phases formed and those contained in raw materials and end products. The different diffractograms corresponding to each formulation were obtained on a D8 DAVINCI apparatus using  $\text{CuK}\alpha$  radiation ( $\lambda = 1.54186\text{\AA}$ ) and a graphite backside monochromator. The analysis range was between  $5^\circ$  and  $50^\circ$  with a step of 0.02 and an acquisition time of 2s. The crystalline phases present in the raw materials and geopolymers were identified using EVA software.

### 2.3.1.4 Fourier transform infrared spectroscopy FTIR

FTIR spectroscopy is an analytical technique based on the absorption phenomenon that occurs when infrared radiation passes through the material. This is then observed selectively, depending on the excited vibrations of the sample. Indeed, each molecule or group constituting the material has vibration levels corresponding to precise energies. When the molecule is excited at its own vibration energy, it absorbs the incident energy, thus allowing the study of the different bonds present in the material. Infrared spectroscopy measurements are carried out in transmittance mode before being processed in absorbance mode by a spectrometer such as the "Thermo Fischer Scientific Nicolet 380". The pellets were obtained by making a well-milled mixture containing 0.1 g of KBr and a fine quantity of material powder, the whole being introduced into a cell and pressed up to 10 tons. The resulting pellet was placed in the apparatus for characterization. Acquisitions were recorded between  $500\text{ cm}^{-1}$  and  $4000\text{ cm}^{-1}$ . The number of scans was 64 and the resolution  $4\text{ cm}^{-1}$ . The OMNIC software is then used for data acquisition and processing. In order to eliminate the contributions of  $\text{CO}_2$  from the air present on each spectrum, these are corrected by a straight line between  $2400$  and  $2280\text{ cm}^{-1}$ .



### 2.3.2 Physico-chemical and mechanical properties

#### 2.3.2.1 Water absorption, Apparent porosity, and Bulk density

Water absorption, apparent density, and apparent porosity are characteristics that permit to evaluated the physical parameters of samples. There have been calculated according to the standard ASTM C373-88. The samples were firstly dried in an oven at 105°C 24h until the mass constant ( $M_1$ ). After that, the samples have been impregnated in water for another 24h. Then, saturated mass ( $M_2$ ), and suspended mass ( $M_3$ ) have been determined. The physical properties are obtained using the following equations (1), (2), (3) respectively for water absorption (WA), apparent porosity (AP), and bulk density (BD). This test was carried out according to ASTM standard [32].

$$WA = \frac{M_2 - M_1}{M_1} \times 100 \quad (1)$$

$$AP = \frac{M_2 - M_1}{M_2 - M_3} \times 100 \quad (2)$$

$$BD = \frac{M_1}{M_2 - M_3} \times \rho(\text{water})$$

#### 2.3.2.2 Flexural strength

Flexural strength  $\sigma$  represents the ability of a material to bending stress. The different values of strength have been obtained using equation (4).

$$\sigma = \frac{3Fd}{2le^2} \quad (4)$$

$\sigma$ (MPa),  $e$  (mm),  $l$ (mm),  $F$ (N)

### 2.3.3 Mercury intrusion porosimetry and Microstructural characteristics

After measurements of flexural strength, some fragments were collected for the microstructural observation using an Environmental Scanning Electron Microscope. The others for the (MIP) analysis.

#### 2.3.3.1 Mercury intrusion porosimetry

Pieces collected from different formulations after the three-point bending test were used to prepare specimens for the MIP (AutoPore IV 9500 V1.09) tests using 1 high-pressure analysis port (33,000 psia maximum pressure) and 2 low-pressure analysis ports. Each specimen was put in a penetrometer with 15 mL sample cup and steam volume of 1.1 mL

(The steam volume depends of the penetrometer used for this study used one with steam volume 1.1). The total pore volume was evaluated using the set-time equilibrium (10 sec) mode between pressure limits of 345 kPa and 228 MPa covering the pore diameter range from approximately 0.0055 to 360  $\mu\text{m}$ .

### 2.3.3.2 Environmental Scanning Electron Microscope

The Environment Scanning Electron Microscope (ESEM, Quanta200, FEI) was adopted as the most suitable technique for the study of the morphology of both metakaolin and meta-halloysite-based geopolymer products with the advantage that the relative humidity can be controlled by both the water vapor pressure and the temperature in the ESEM-chamber. This observation approach permits avoiding the influence of cracks from the drying process necessary when the high vacuum SEM is used.

## 3. Results and discussion

### 3.1 Characterization of raw materials

#### 3.1.1 Fluorescence X-ray analysis

Table 2: Chemical compositions of raw laterite, rice husk ash, and fine quarry sand.

Oxides (wt. %)	Raw Laterite (LAT)	Rice husk ash (RHA)	Fine Quarry sand (QS)
Al <sub>2</sub> O <sub>3</sub>	17.93	0.52	16.33
SiO <sub>2</sub>	25.30	87.01	53.87
P <sub>2</sub> O <sub>5</sub>	0.18	1.03	0.25
S <sub>3</sub> O	0.05	0.18	1.09
K <sub>2</sub> O	0.12	3.03	2.68
CaO	0.07	0.58	2.18
TiO <sub>2</sub>	1.21	/	1.73
Fe <sub>2</sub> O <sub>3</sub>	41.28	0.50	15.10
Na <sub>2</sub> O	/	/	1.17
MgO	/	/	3.81
MnO	/	/	0.27
Others	0.38	0.55	0.12
L.O.I (loss on ignition)	13.48	6.60	1.40
Al/Si	0.83	0.01	0.36

The chemical compositions of laterite, fine quarry sand and rice husk ash (RHA) are tabulated in Table 2. It is observed that laterite is composed of 41.28 % of Fe<sub>2</sub>O<sub>3</sub>; 25.30 % of SiO<sub>2</sub> and 17.93 % Al<sub>2</sub>O<sub>3</sub> as major oxides. These major oxides are well known as good precursor of geopolymer binders suggesting that laterite is suitable for the synthesis of inorganic polymer cements [19]. Fine quarry sand is mainly constituted of 53.90 % of SiO<sub>2</sub>, 16.33 % of Al<sub>2</sub>O<sub>3</sub> and 15.10 % Fe<sub>2</sub>O<sub>3</sub>; with low percentages of MgO (3.80%), CaO (2.20 %) and K<sub>2</sub>O (2.70%). Rice husk ash (RHA) used as reactive silica source is mainly composed of

87,01 % of SiO<sub>2</sub>. The laterite used in this study present a sum of Al<sub>2</sub>O<sub>3</sub>+Fe<sub>2</sub>O<sub>3</sub>+SiO<sub>2</sub>= 85wt% largely>80wt% recommended for the solid precursor of geopolymers [19]. Moreover, the amount of kaolinite is 36wt% (major fraction with disordered structure due to the corrosion of kaolinite by iron minerals). This clayey material with high potential reactivity in alkaline solution is accompanied with 31 wt% of goethite knowing for their good reactivity in the presence of soluble silica [19, 25, 33, 34]. This justifies the use of rice husk ash which has the role to provide soluble silica into the formulation. Powder sand here is acting as filler for achievement of densified structure.

### 3.1.2 Thermogravimetric analysis

The simultaneous thermogravimetric (TG/DTA) curves of the raw laterite are given in Figure 1. The TG curve shows three endothermic peaks which characterize weight losses recorded at 200, 350, and 650 °C, respectively. The first weight loss of 3% located at 46°C can be attributed to the release of free or physisorbed water. At 270 °C the second endothermic peak corresponds to the dehydroxylation of goethite into hematite followed by 3 % of mass loss recorded on TG curve. Finally, at 478 °C, the third endothermic peak exhibits 5% loss in mass (recorded in TG curve) corresponding to the dehydroxylation of kaolinite into metakaolinite. The peak of the dehydroxylation of kaolinite generally appears in the range of 520-550 °C [19, 35, 36]. This low value recorded on DTA curve can be explained by the fact that the actual laterite is highly corroded by the iron minerals. Therefore, the level of disorder in laterite makes their structure weaker under thermal treatment.

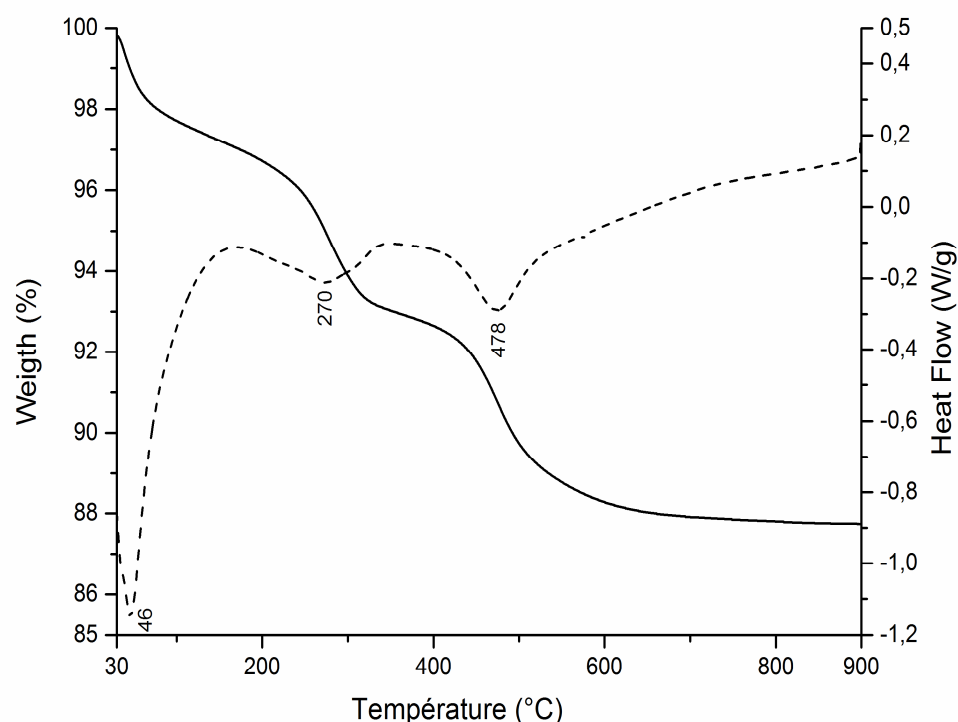
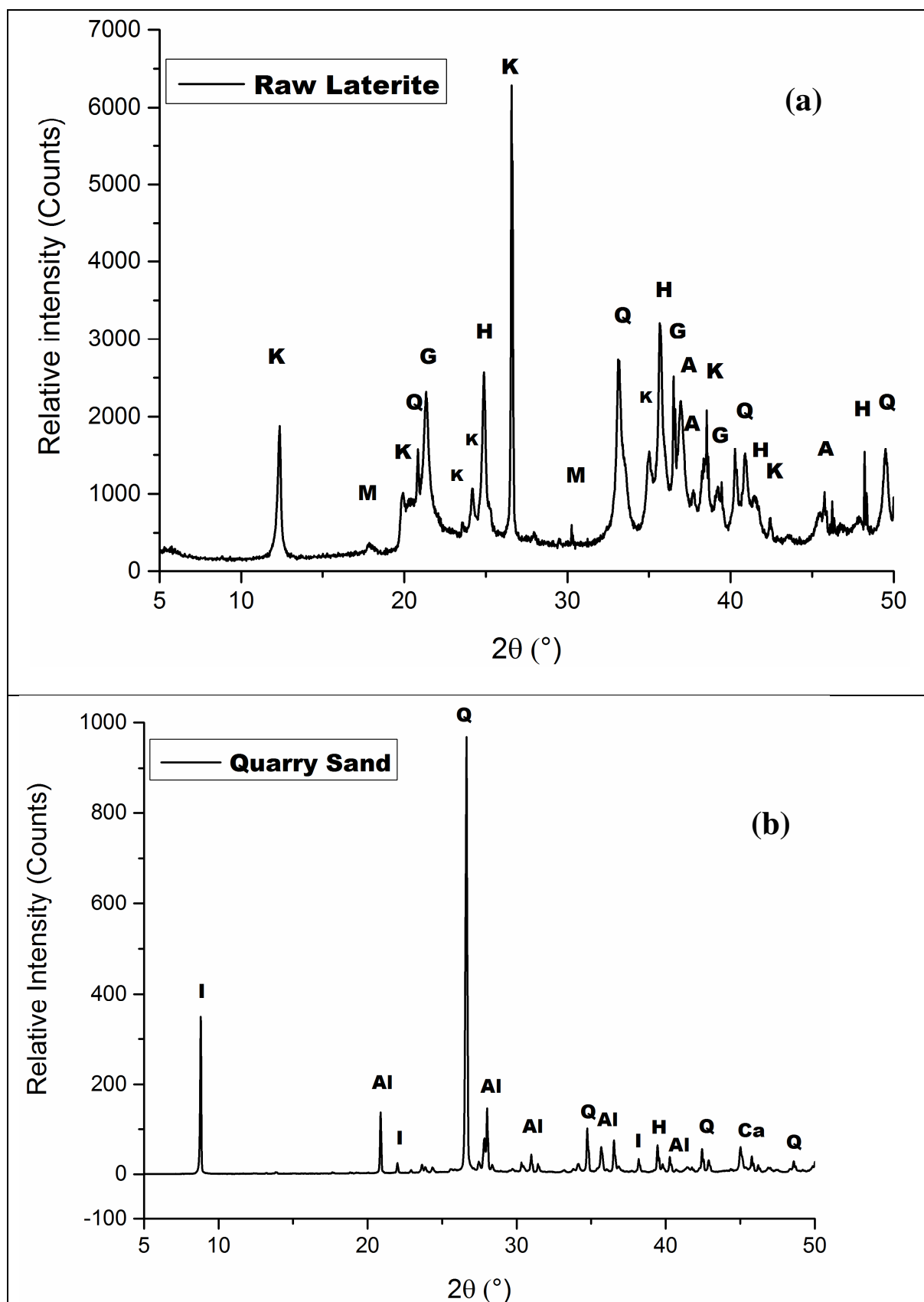


Figure 1. Differential thermal and thermogravimetry analysis of raw laterite.

### 3.1.3 X-Ray Diffraction analysis

The analysis of the different X-ray patterns illustrates the mineralogical phases contained in the raw materials. From Figure 2, the main mineral phases present in the raw laterite are quartz ( $\text{SiO}_2$ , (Q) PDF# 04-006-1757), hematite ( $\alpha\text{-Fe}_2\text{O}_3$ , (H) PDF# 04-015-9569), kaolinite ( $\text{Al}_2\text{Si}_2\text{O}_5(\text{OH})_4$ , (K) PDF# 00-005-0143), goethite ( $\alpha\text{-FeO}(\text{OH})$ , (G) PDF# 04-015-8212), maghemite ( $\gamma\text{-Fe}_2\text{O}_3$ , (M) PDF# 04-021-3968) and anatase ( $\text{TiO}_2$ , (A) PDF# 04-014-0490) (Figure 2a).

The quarry sand contains illite ( $(\text{K},\text{H}_3\text{O})(\text{Al},\text{Mg},\text{Fe})_2(\text{Si},\text{Al})_4\text{O}_{10}[(\text{OH})_2,(\text{H}_2\text{O})]$ , (I) PDF# 04-021-0353), albite (Al) PDF# 00-020-0548), quartz ( $\text{SiO}_2$ , (Q) PDF# 04-006-1757), hematite ( $\alpha\text{-Fe}_2\text{O}_3$ , (H) PDF# 04-015-9569) and calcite ( $\text{CaCO}_3$  (Ca), PDF# 04-020-5889, 04-008-0212) (Figure 2b). Figure 2c highlights the presence of the following mineral phases contained in rice husk ash: quartz ( $\text{SiO}_2$ , (Q) PDF# 04-006-1757), tridymite ( $\text{SiO}_2$ , (T) PDF# 04-012-1133) and cristobalite ( $\text{SiO}_2$ , (C) PDF# 04-012-1126).



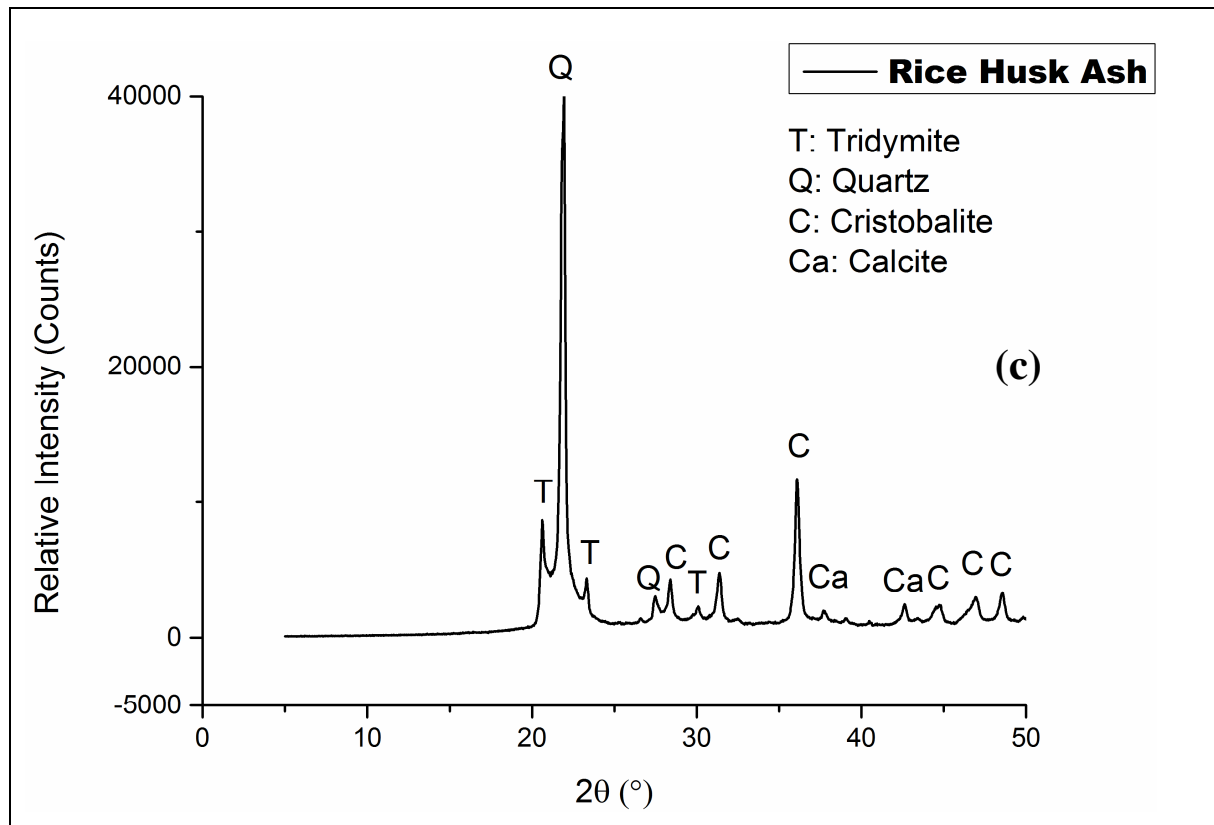
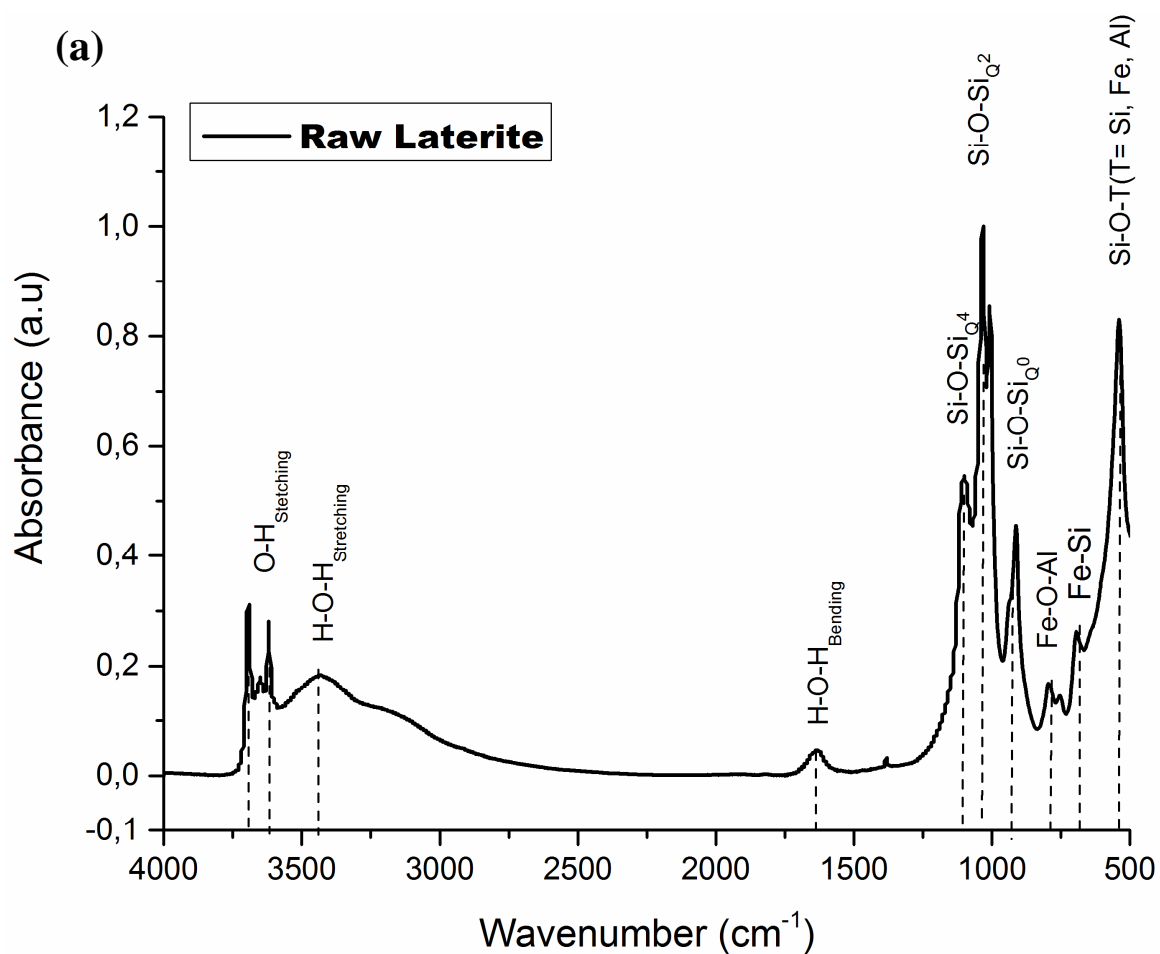


Figure 2. X-ray diffractograms of (a) raw laterite, (b) rice husk ash and (c) quarry sand. PDF files: Q (04-006-1757); H (04-015-9569); G (04-015-8212); K (00-005-0143); M (04-021-3968); A (04-014-0490); I (04- 021-0353); Ca (04-020-5889); C (04-012-1126); T (04-012-1133); Al (00-020-0548).

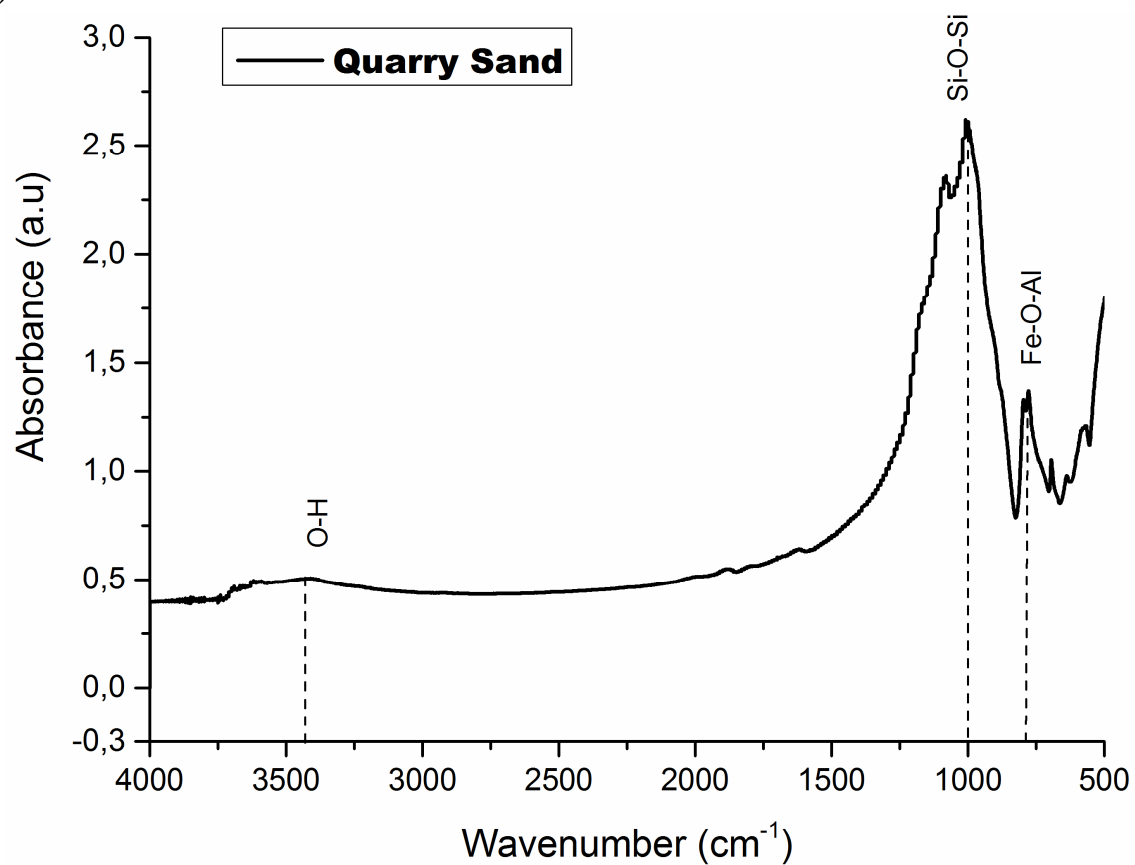
#### 3.1.4 Fourier transform infra-red spectroscopy

Figures 3 exhibits the infrared spectra of laterite, rice husk ash, and quarry sand respectively. These infrared spectra reveal several important absorption bands. The first bands between 3700-3600  $\text{cm}^{-1}$  indicates the presence of H-O stretching bonds linked to Al-OH and Fe-OH belonging to kaolinite and goethite respectively [2, 3, 19]; the second bands at 3450 and 1630  $\text{cm}^{-1}$  are attributed to the H-O stretching and bending bonds of water molecules respectively, the third bands between 1100 and 918  $\text{cm}^{-1}$  are attributed to the Si-O-M bonds (M= Si, Al, and Fe) the fourth band at 794  $\text{cm}^{-1}$  is related to the Fe-O-Al bond and the last band bands between 538-476  $\text{cm}^{-1}$  are assigned to the Fe-O-Si bonds corresponding to the vibrating bonds of goethite and hematite [19, 23, 25, 35]. The rice husk ash spectrum (Figure 3b) shows the absorption bands at 1101, 985 and 694  $\text{cm}^{-1}$  which correspond respectively to Si-O-Si ( $Q^3$ ,  $Q^2$  and  $Q^0$ ) [37, 38]. Figure 3c describes the infrared spectrum of quarry sand. It shows three main bands, the first band at 3490  $\text{cm}^{-1}$  is attributed to the O-H stretching, the

319 second band located at  $1080\text{ cm}^{-1}$  is linked to the vibration mode of Si-O-Si bond. The last  
 320 band appearing at  $796\text{ cm}^{-1}$  is attributed to the Fe-O-Al bonds [3, 7, 20, 35, 39].



(b)





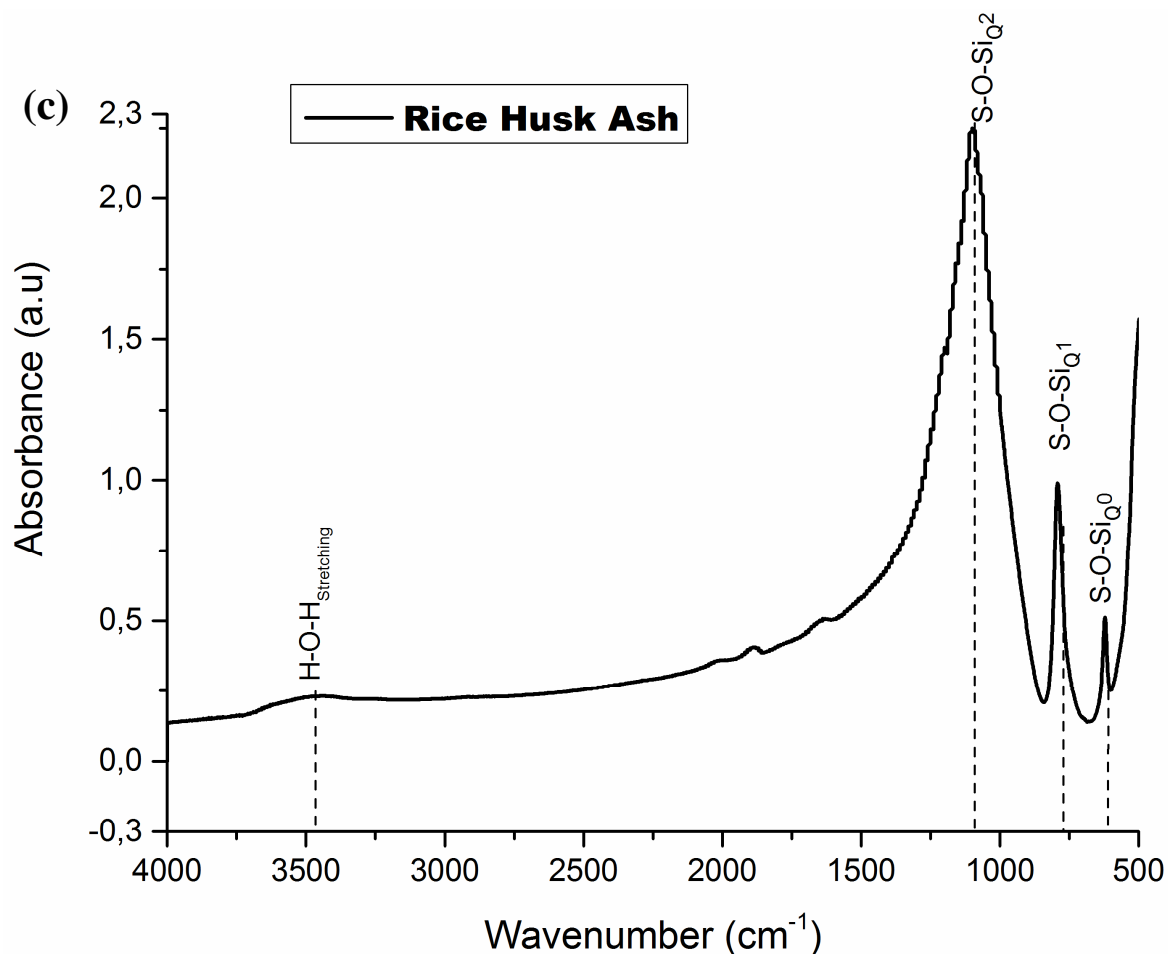


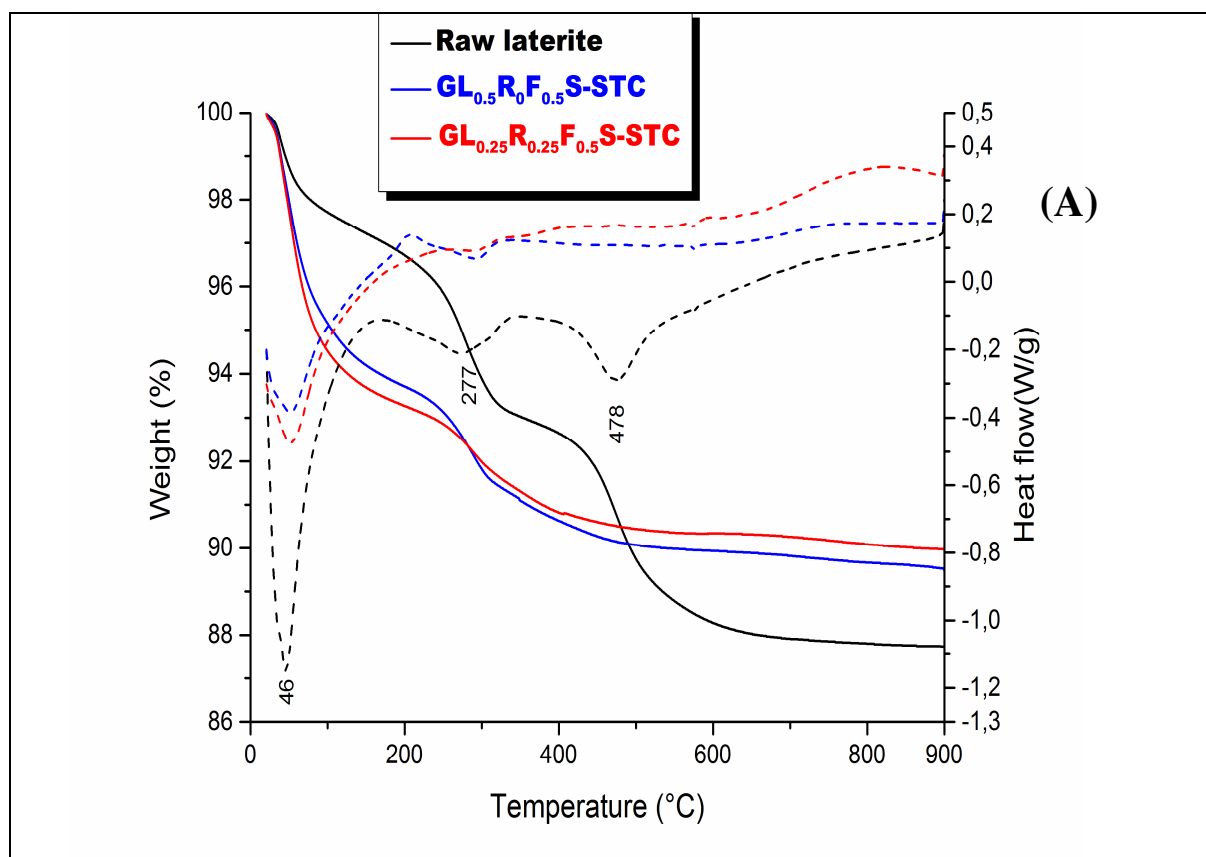
Figure 3. FTIR spectra of (a) raw laterite, (b) quarry sand and (c) rice husk ash.

## 3.2 Characterisation of geopolymer composites

### 3.2.1 Phases evolution

Figure 4 highlights the simultaneous TG-DTA curves exhibiting the behavior of geopolymer composites undergone at different curing cycles: (a) steam curing chamber (STC), (b) room temperature curing (RTC) and (c) outside curing temperature (OTC). From Figure 4, the TG curves are represented in solid lines and the DTA curves in dashed lines. These curves of geopolymer composites show a unique important endothermic peak appearing at 46°C. This endothermic peak is linked to free water present in the geopolymer matrix. The geopolymer matrix is generally considered as a hydrophobic material with capacity to fix instantly the humidity. This humidity is removed as soon as the temperature is higher respecting the standard room temperature. The small endothermic peak presents at 277 °C suggests the residual goethite mineral compound that did not participate to the reaction of geopolymerization. Conversely, the dehydroxylation peak of kaolinite has completely

disappeared during the reaction, demonstrating the complete reactivity of kaolinite. Apart from the weight loss due to the physisorbed water (7%) and that of the goethite (2%), the matrix of geopolymer composites remains stable up to 900°C. This behavior is in agreement with the finding of the literature [19,25]. When applied oven and ambient temperature curing (RTC), the geopolymer sample exhibits an endothermic peak at 573 °C which is attributed to the  $\alpha$ ,  $\beta$  quartz transformation [37]. In case of RTC or OTC, the final product of geopolymerization still exhibit quartz grains under thermal treatment (Figure4b, c). While with steam curing, no evidence of quartz was observed (Figure 4a). The possible interpretation is to suggest the surface dissolution of quartz occurred when the temperature of 80°C is combined with high level of humidity. Thus, enhancing the chemical bond development between quartz and geopolymer gel contributing to the densification of geopolymer composite structures [28, 40].



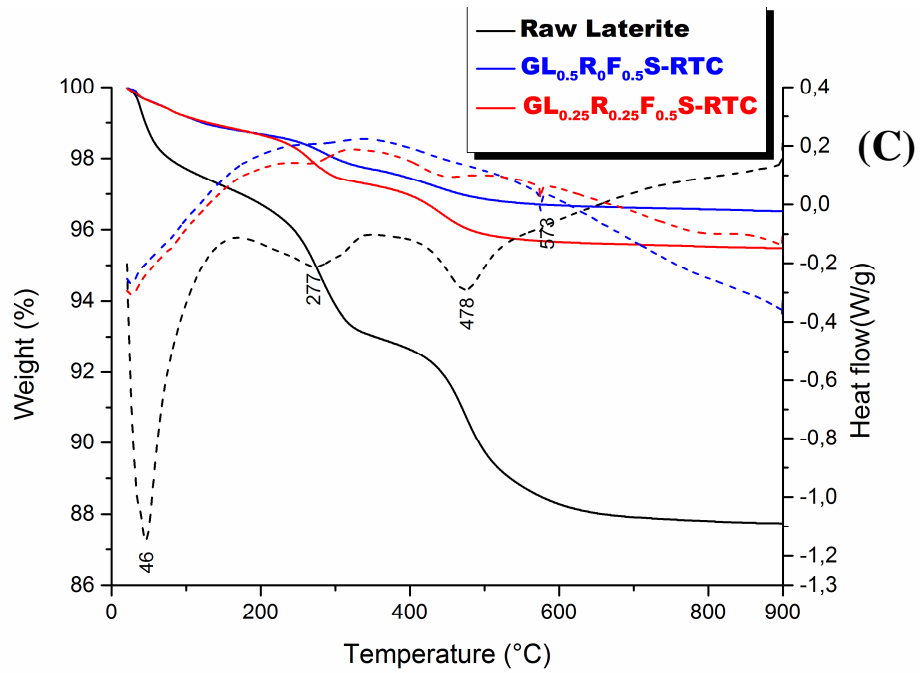
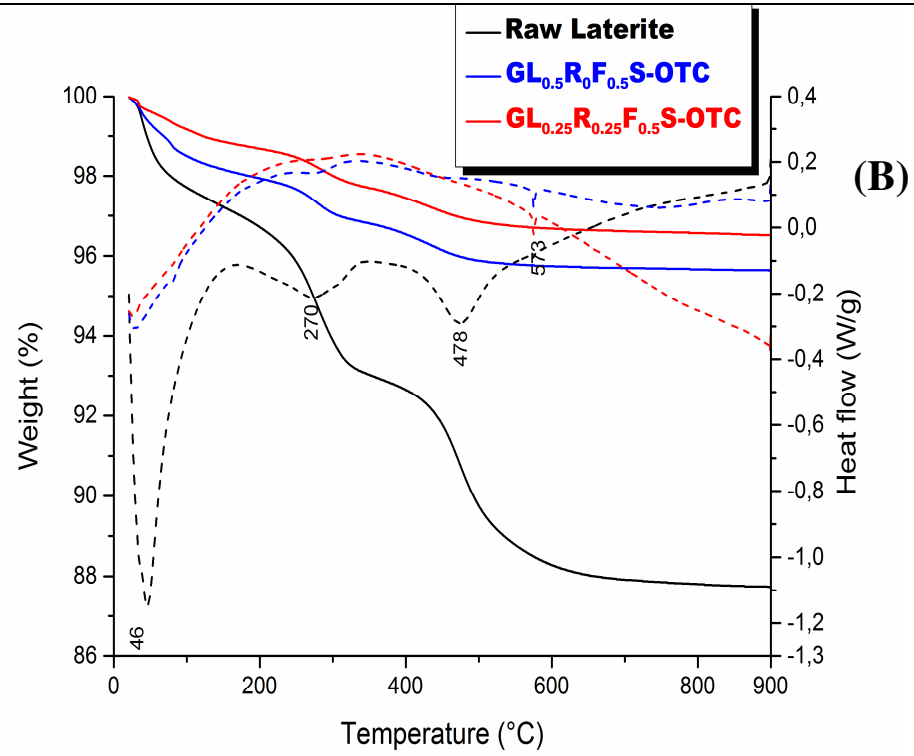
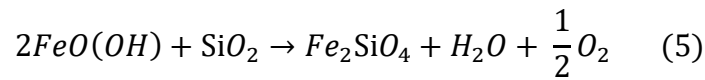
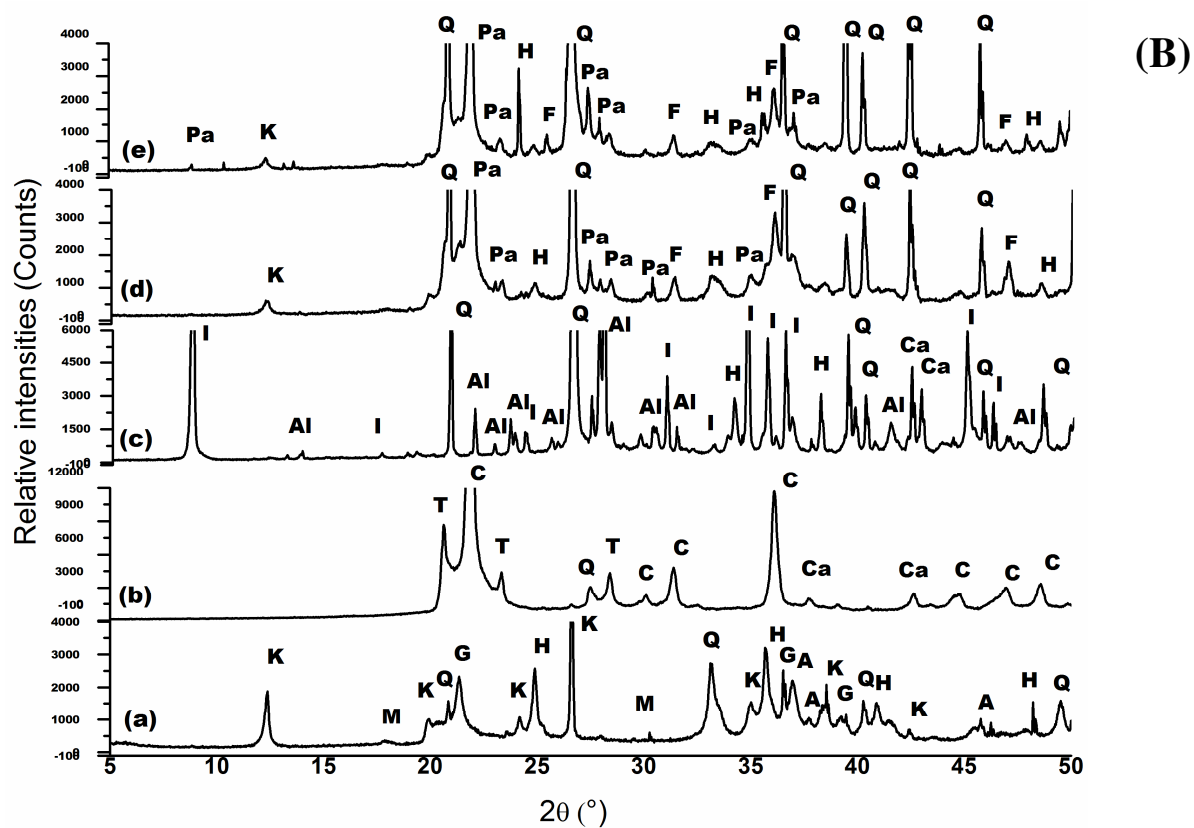
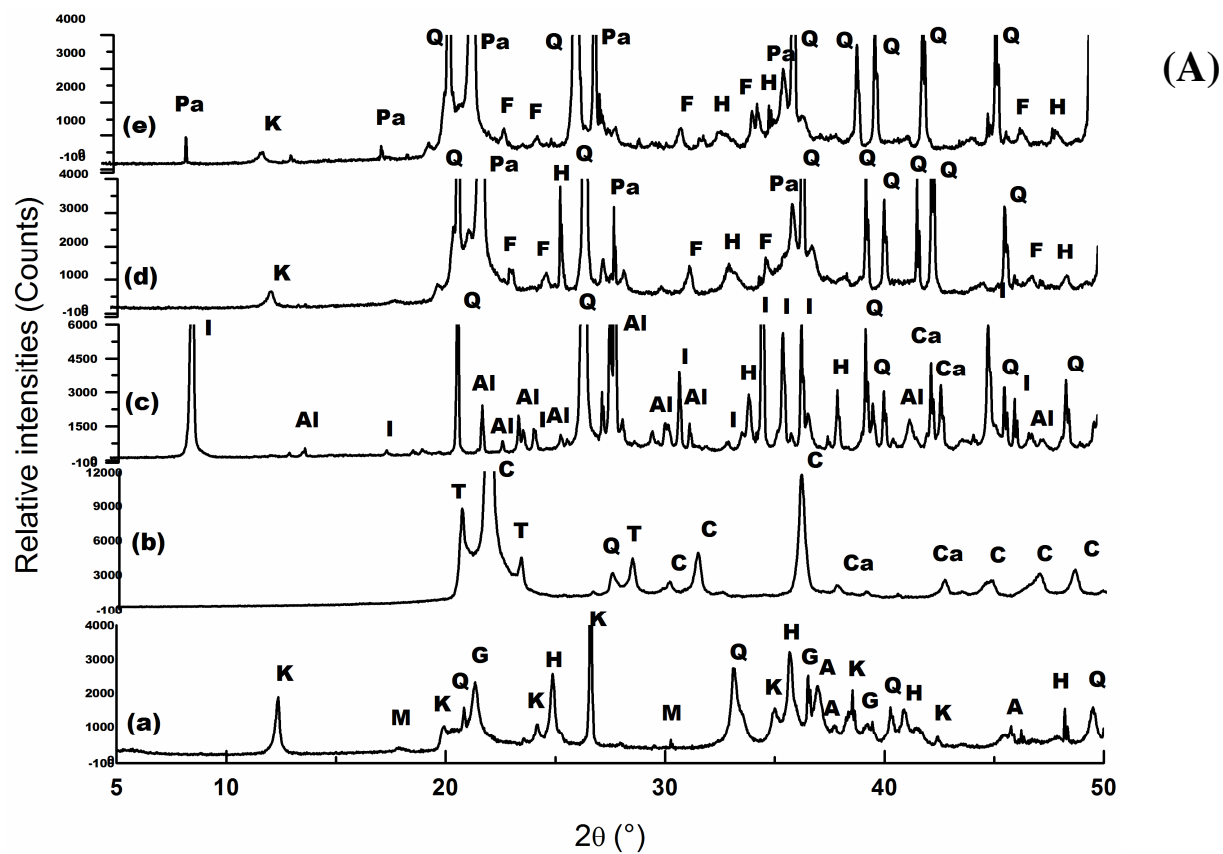


Figure 4. Superimposed TG/DTA curves of raw laterite and geopolymer composites under different curing cycles: (A) STC, (B) OTC, and (C) RTC.

Figure 5 presents the X-ray patterns of raw laterite, rice husk ash, quarry sand, and geopolymer composites. It is noticed that the more pronounced reflection peaks of kaolinite and goethite in raw laterite diminished in terms of intensity on the diffractograms of laterite-based geopolymer composites after consolidation with alkaline solution (Figures 5a, 5b, and 5c). This reduction clearly shows that the kaolinite mineral in corroded laterite is in disordered state as reported by Kaze et al [25], thus enable to react in contact of alkaline solution. However, the presence of (quartz and hematite) contained in raw laterite also appeared on XRD of formed products, indicating that they were not totally altered during the geopolymerization reaction. The disappearance of goethite mineral after alkaline activation is linked to the reaction that occurs between goethite and silica species during the geopolymerization reaction leading to formation of iron silicate compounds like fayalite and hinsingerite detected on the XRD of geopolymer composites. The formation of fayalite is explained by equation (5).



Similar observations were done by other researchers [7, 19, 25] who showed that increasing the curing temperature between 25 and 200 °C allows the formation of iron silicate compounds like fayalite, hinsingerite which reinforced the geopolymer structure and improved the strength [7, 25]. As seen on the X-ray patterns of different consolidated specimens, the rise of curing temperature depending on curing cycles did not affect the formation of phases during the geopolymer process.



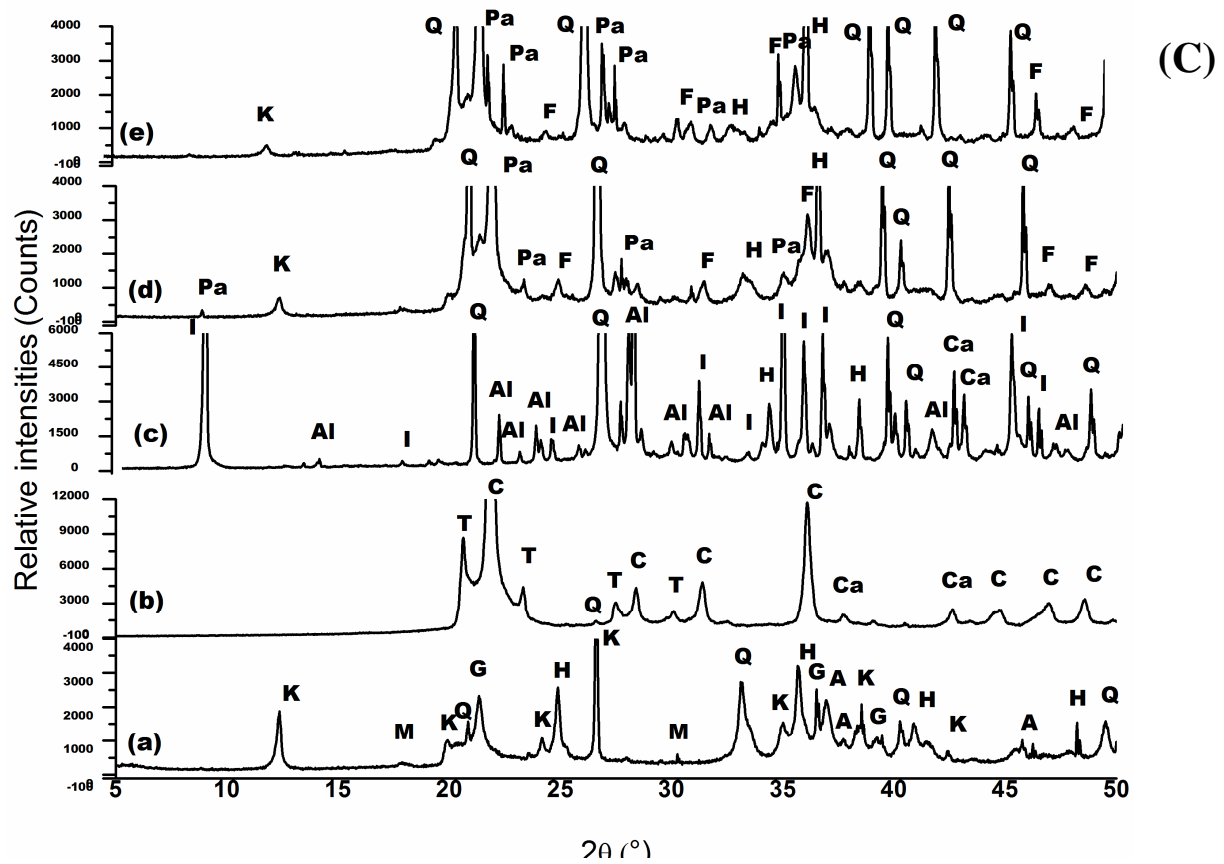
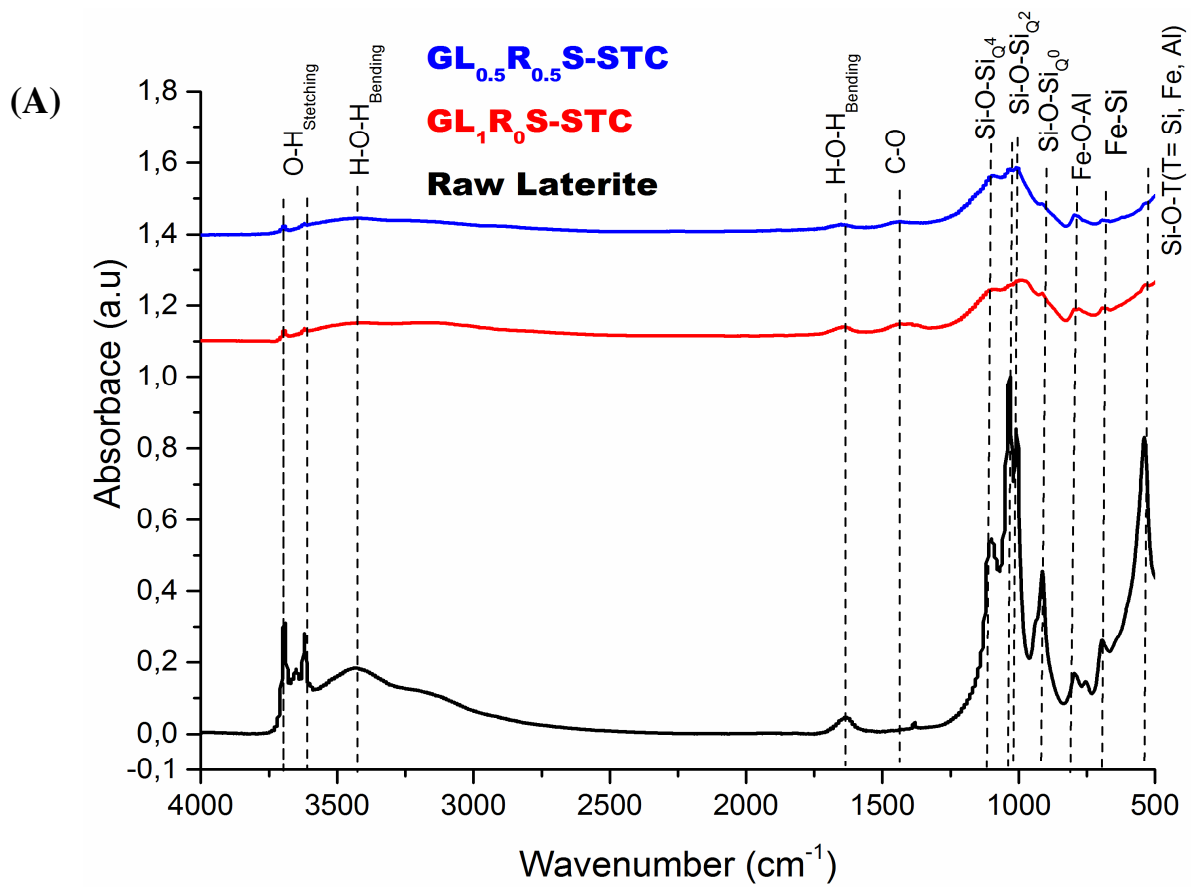
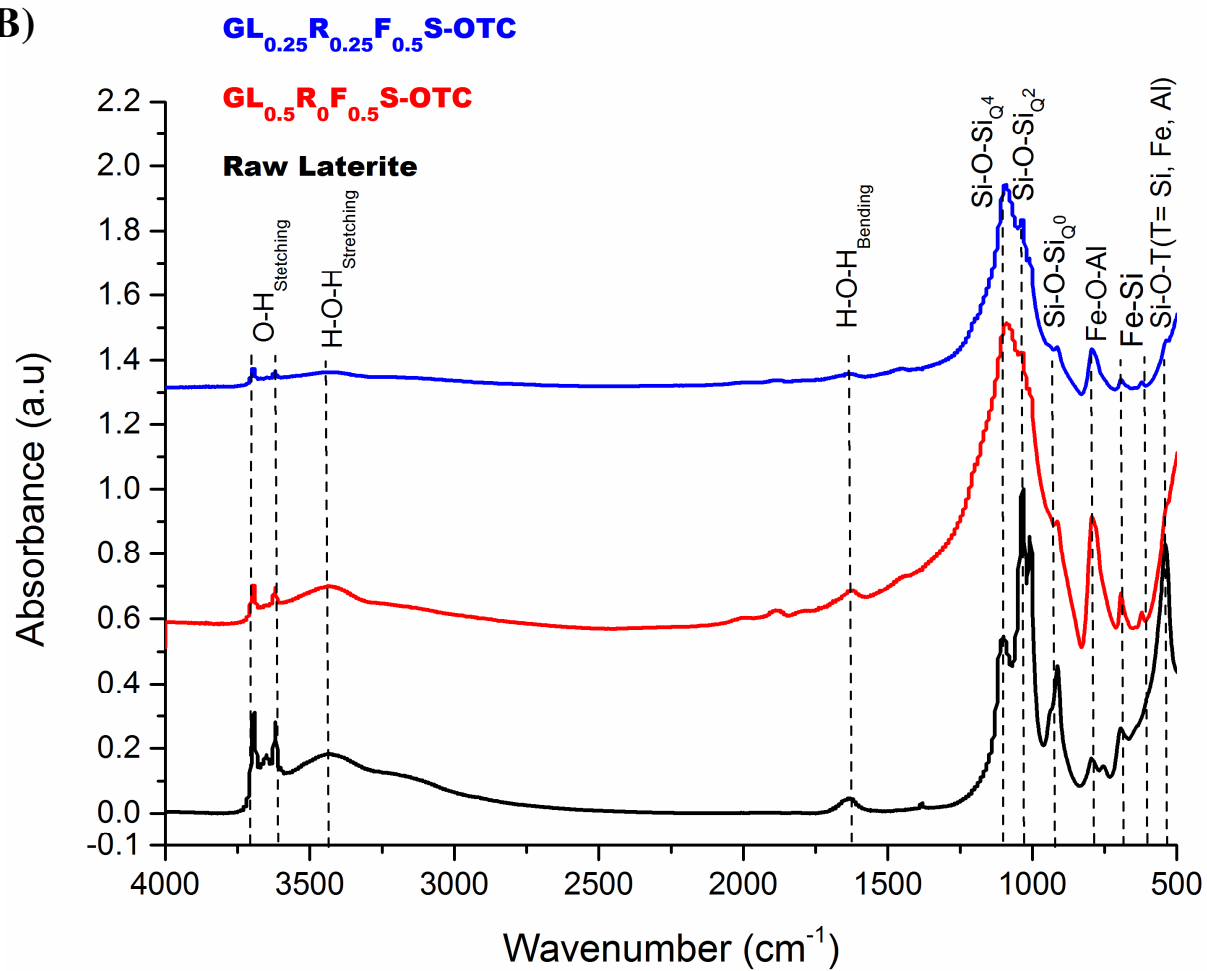


Figure 5. X-ray diffractograms of raw laterite, rice husk ash, quarry sand and GL<sub>1-Y-Z</sub> R<sub>Y</sub>F<sub>Z</sub>S (A) STC, (B) OTC, and (C) RTC. PDF files: Q (04-006-1757, 04-008-7652, 04-008-2359, 04-008-7651); H (04-015-9569, 04-018-0098, 04-010-3230, 04-008-8479); G (04-015-8212); K (00-005-0143); M (04-021-3968, 04-009-9615, 04-016-4344); A (04-014-0490, 04-014-8515); I (04-017-0518), F (04-008-8542, 04-007-5852) Pa (04-015-9389).

Figure 6 exhibits the superimposed infrared spectra of raw laterite, GL<sub>1</sub>R<sub>0</sub>S, and GL<sub>0.5</sub>R<sub>0.5</sub>S geopolymer composite specimens. From Figure 6, it can be observed that the absorption bands located at 3696, 3622, 3423, and 1630 cm<sup>-1</sup> corresponding respectively to H-O<sub>kaolinite</sub>, H-O<sub>goethite</sub>, H-O-H<sub>stretching</sub> and H-O-H<sub>bending</sub> have considerably decreased on the spectra of the synthesized laterite-based geopolymer composite materials [19]. This reduction in absorbance peaks belonging to kaolinite and goethite indicates that these minerals have taken part in geopolymerization reaction showing the structural disorder of kaolinite in laterite as reported by Obonyo, et al. [41], Kamseu, et al. [7] and Kaze, et al. [19]. The absorption bands present at 1442 cm<sup>-1</sup> on GL<sub>1</sub>R<sub>0</sub>S-STC and GL<sub>0.5</sub>R<sub>0.5</sub>S-STC spectra are attributed to vibrational mode of C-O bond. This band is formed from the reaction between Fe that migrated out of geopolymer matrix and CO<sub>2</sub> from the atmosphere as it has been found by Kaze et al. [2] and Nkwaju et al. [23].



(B)



386



(C)

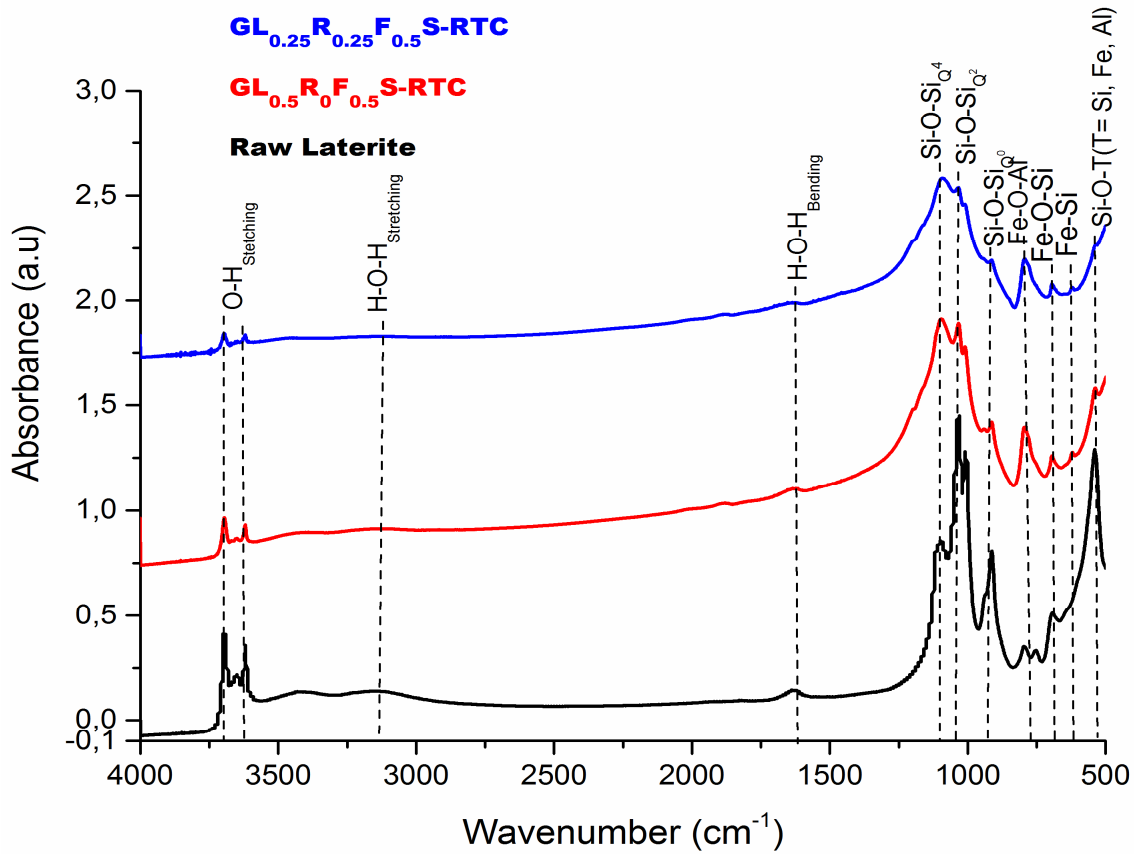


Figure 6. Infrared spectra of raw laterite,  $GL_{1-y-z}R_yF_zS$  (A) STC, (B) OTC, and (C) RTC.

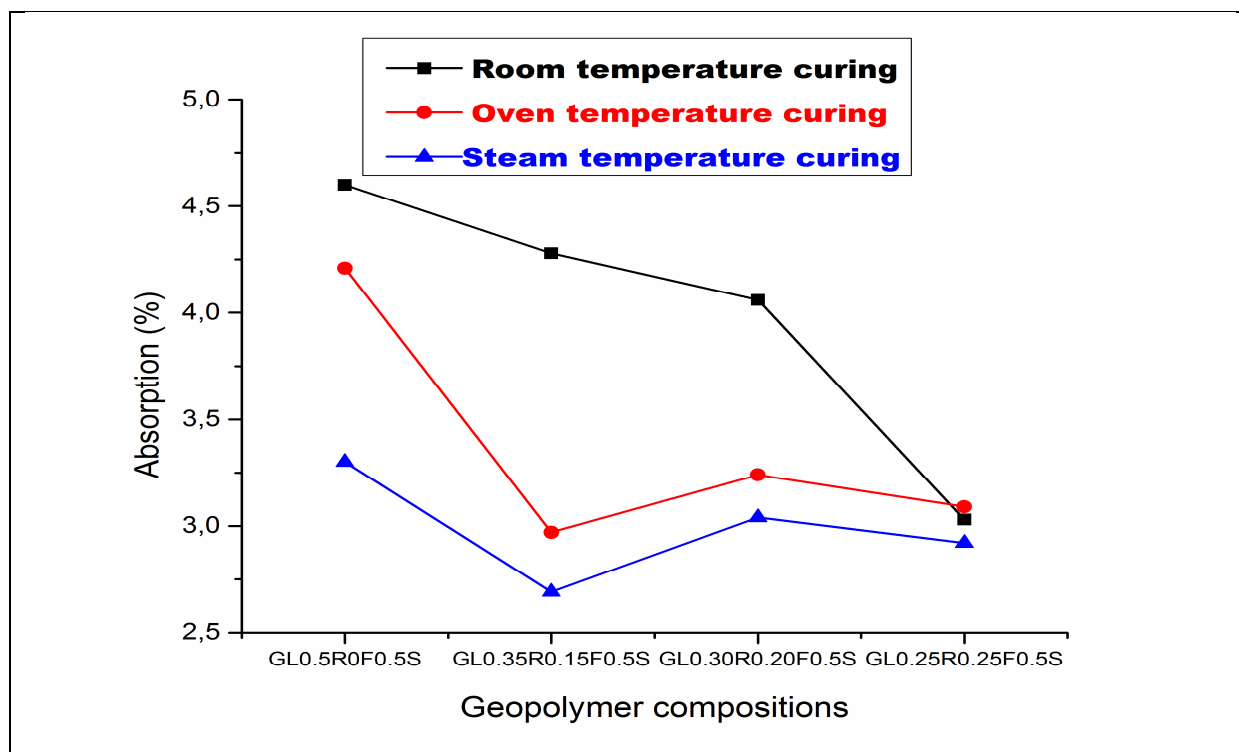
### 3.2.2 Water absorption, apparent porosity, and bulk density

The values of water absorption, apparent porosity and bulk density are presented in Figure 7, 8 and 9 respectively. The values of water absorption recorded on  $GL_{1-y-z}R_yF_zS$  specimens cured at room temperature (RTC), oven curing (OTC) and steam curing (STC) are 4.60, 4.28, 4.06 and 3.03%; 2.70, 4.21, 3.24 and 3.09 % and 3.30, 2.70, 3.04 and 2.92 %, respectively for the samples containing 0, 15, 20 and 25% of rice husk ash (Figure 7). It is observed that the curing cycle does not significantly affect the water absorption. The lower values recorded on different specimens independently of the curing modes exhibit the better compact matrix with few accessible pores or voids that could allow the retention in water content when samples are soaked in water for the water absorption test. In addition, the use of reactive silica from rice husk ash in the whole matrix allowed the formation of Si-O-Al and Si-O-Fe bonds leading to the formation of polysialate and polyferrisialite binder phases that improved and made the strong matrices, ensuring the high mechanical performances achieved. In the same approach Kamseu et al. [7] showed that the densification of laterite-based geopolymer composite replaced by rice husk ash up to 25 wt% is due to the formation of iron silicate minerals like hinsingerite.

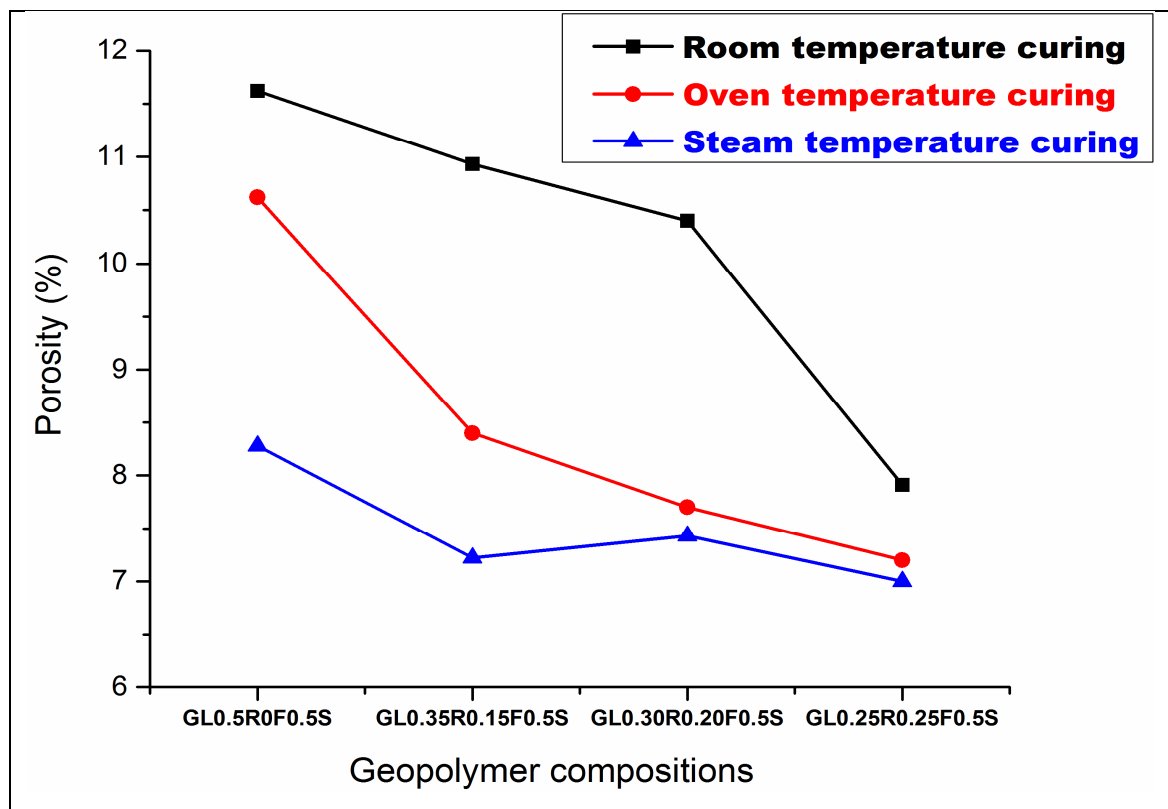
For  $GL_{1-y-z}R_yF_zS$  geopolymer specimens cured at room temperature (RTC), the decreased values of apparent porosity are 11.62, 10.93, 10.40, and 7.91 %, containing respectively 0, 15, 20, and 25 wt% of rice husk ash (Figure 8). When oven curing (OTC) and steam curing (STC) are used, these values are 6.70, 10.62, 8.06, 7.34 %, and 8.28, 7.22, 7.43, and 7.00 %, respectively. The reduction in apparent porosity with increase in rice husk ash content when applying room temperature curing (RTC) could likely due to the high concentration of Si-monomers from dissolution of reactive silica from RHA in alkaline medium that help to reduce the formation of the voids and pores within the geopolymer composite matrices. The lower percentages recorded on other curing types (OTC and STC) could be either due to (i) formation of iron silicate minerals from silica and iron compounds resulting in an improvement of structure or (ii) hydrosodalite formed from residual kaolinite in metastable nature contained in laterite with alkaline solution leading to an extension of binder phase, reinforcing the matrix. This is in accordance with the findings of Kaze et al. [25] where the authors concluded that the reduction in apparent porosity with increase in curing temperature was linked to the formation of iron silicate phases that made the geopolymer matrix dense and compact.

In the case of bulk density, the values obtained for  $GL_{1-y-z}R_yF_zS$  samples according to the different curing types RTC, OTC and STC were 2.45, 2.52, 2.54, and 2.60 g/cm<sup>3</sup>; 2.49, 2.54, 2.56, and 2.69 g/cm<sup>3</sup> and 2.50, 2.61, 2.67 and 2.86 g/cm<sup>3</sup> respectively for the samples containing 0, 30, 40, and 50% of rice husk ash (Figure 9). These similar values are linked to the better cohesion between different phases present in the developed geopolymer microstructure. The high values in terms of bulk density compared to that of standard metakaolin-based geopolymers could be linked to the low quantity of kaolinite and hematite that did not react during the geopolymer process and made the samples a bit heavy as reported by Kaze, et al. [25]. Taken into account the physical results, it can be shown that the effect of curing type is more observed with the porosity where the values decrease according in range RTC, OTC, and STC. Finally, the increase in bulk density recorded on all the geopolymer composite samples made with RTC, OTC and STC cycles is likely linked to the progressively formation of strong matrix which occurred with the increase of rice husk ash leading to few accessible voids. The lower values in bulk density recorded on samples made with RTC and OTC curing modes compared to STC one can be explained by the defects such as open voids and micro-fissures occurring in the matrix when the humidity is not controlled. Hence with the lower porosity and water absorption, laterite-based geopolymers made with STC cycle expected to have high bulk density as shown in Figure 9. This could be due to the better

438 cohesion among geopolymer binder and aggregates with lower voids that could retain water  
 439 when samples are immersed for water absorption and porosity tests.



440 Figure 7. Water absorption of geopolymer composites subjected in different curing cycles.



441 Figure 8. Apparent porosity of geopolymer composites cured in different curing cycles.

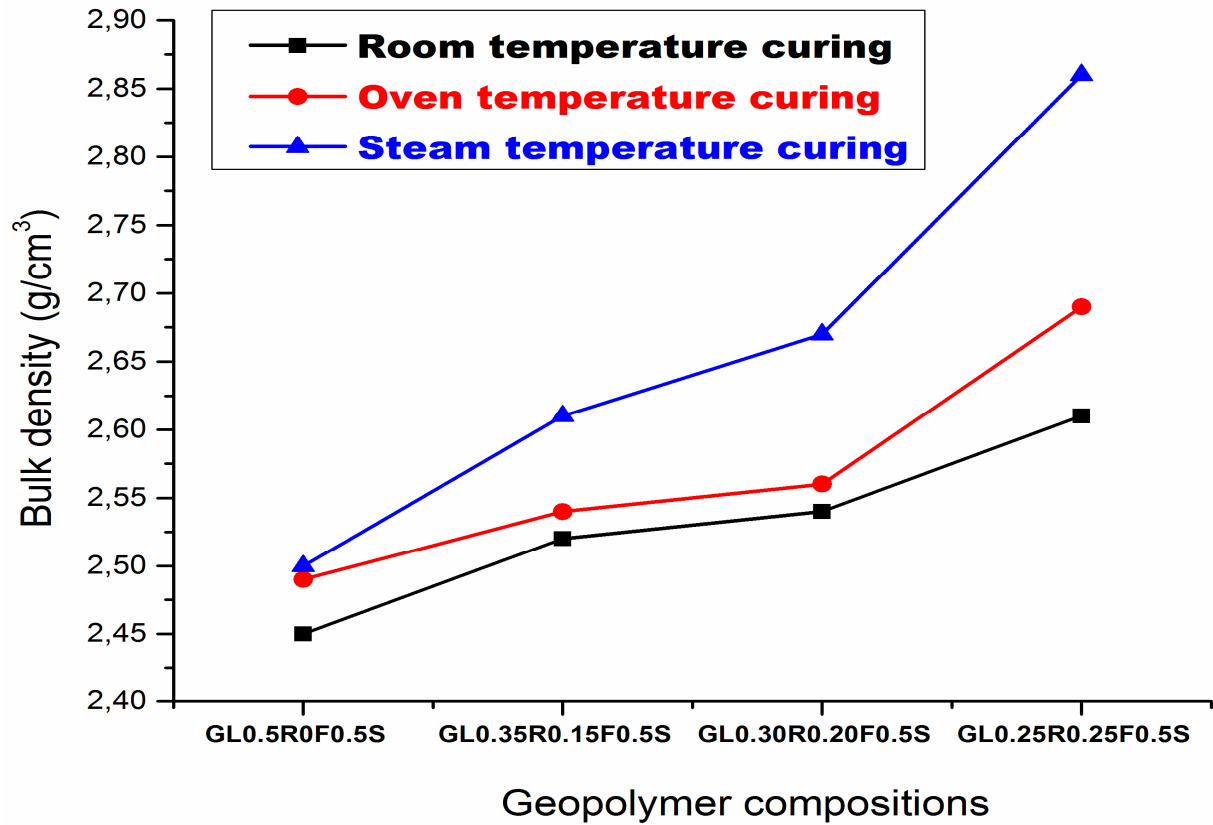


Figure 9. Bulk density of geopolymer composites cured in different curing cycles.

### 3.2.3 Mechanical properties

Figure 10 presents the flexural strength of geopolymer composites namely  $GL_{1-y-z}R_yF_zS$ . For the samples cured at room temperature (OTC), the 28 days flexural strength are 8.35, 14.23, 15.40, and 16.89 MPa respectively for laterite based geopolymer composites containing 0, 15, 20 and 25 % of rice husk ash (RHA). The increase in flexural strength from 8.35 to 15.40 MPa with increasing of RHA up to 20 %, is linked to the release of Si-oligomers from dissolution of reactive silica from rice husk ash that polymerized with iron and aluminium resulting in good polycondensation. The low increase of strength from 15.40 to 16.89 MPa observed after adding 20 and 25 % of RHA is likely due to the fact that the whole system became richer in Si-oligomers. It is well known in the literature that when geopolymer matrix is saturated with Si-O-Si instead of Si-O-Al bonds, lower strength development is expected. In addition, this strength development recorded on samples cured at room temperature once more helps to show that kaolinite within iron-rich laterite is not in pure crystalline nature, thus has partially dissolved in alkaline solution. When consider the room temperature curing, the humidity is easily controlled but the temperature seems not to be enough for the efficient reactivity of iron minerals. In case of oven curing, the earlier

evaporation of water is responsible for the development of interconnected pores with the limitation of the reactivity of iron minerals. It is expected that, the control of the humidity at 80°C favouring the reactivity of iron minerals, will improve the dissolution motivated by disordered nature of kaolinite present in raw laterite. This results in densification of the geopolymer matrices and high mechanical strength achieved.

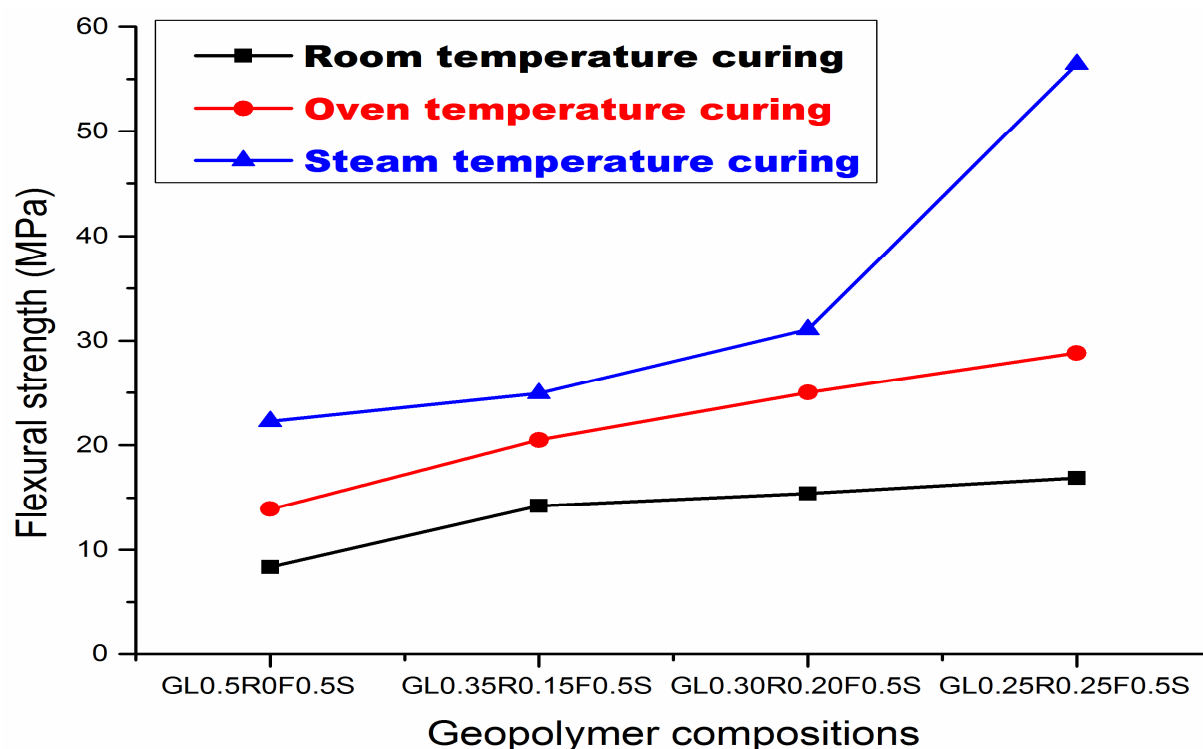


Figure 10. Flexural strengths of geopolymer composites cured in different curing cycles.

When the laterite-based geopolymer composites were oven cured at 80 °C without humidity control, the flexural strength of samples labelled  $GL_{1-y}R_yS$  are 13.9, 20.5, 25.01, and 28.81 MPa, with 0, 15, 20, and 25 % of RHA, respectively, Figure10. The increase in mechanical performance recorded on these samples could be due to the formation of ferrisilicates compounds. This extends the binder phases and reinforces that laterite-based geopolymer composite matrices with compact and dense structure that justify the high strength achieved. The formation of this iron silicate phase in the geopolymer composite matrix is expected to densify the latter, making it stronger as observed in Figure10.

It seems that the temperature of 80 °C applied in the presence of high relative humidity (Steam curing) enhances both the dissolution of the solid precursors and the formation of ferrisilicates as shown in Figures 5, 6, and 10. Steam curing at 80 °C with 65 % of relative humidity the following values of flexural strength recorded on geopolymer composites samples: 22.25, 23.92, 31.06, and 56.41 MPa for the samples with 0, 15, 20, and 25 % of RHA added. This trend shows the importance of water through in controlled humidity in this

curing type that contributed in optimization of geopolymerization reaction. The abrupt release of water molecules in oven curing mode (room temperature and oven curing) affects the strength development in the same formulations justifying the difference observed. This observation matches with those of Dimas, et al. [42], El-nagga, et al. [43], and Park et al. [44] who claimed that the presence of water strongly contained in small voids and pores on the geopolymer binder. Thus, this water is necessary for the stability or equilibrium of geopolymer network leading to non-appearance of microcracks or fissures which could limit the strength development. This behavior matches with the findings of Gallup, et al. [33, 34], Kaze, et al. [25] and Kamseu, et al. [7] who claimed that the iron silicate compounds are formed when combined reactive iron minerals such as goethite and reactive silicate in alkaline media cured between 50 and 200 °C. The hypothesis of the improvement of the dissolution of solid precursor at high relative humidity as well as the important formation of ferrisilicate are in line with the finding of Gallup [33]. The good polycondensation justifies the development of a strong matrix (Figure 10),

#### 3.2.4 Microstructure

Figure 11 presents the microstructure of geopolymer composites containing 0, 15 and 25% of rice husk ash that have undergone OTC curing cycle. From Figure 11a, the micrographs of geopolymer composites without rice husk ash exhibit an inhomogeneous structure with microcracks and porosity along their matrices. The presence of the open voids and porosity could be due to the low value of  $\text{Si}/\text{Al}=1.20$  and  $\text{Si}/\text{Fe}=0.82$  ratios [25]. In general the  $\text{Si}/\text{Al}=2$  and  $\text{Si}/\text{Fe}>1$  are required for the high polycondensation favouring the development of a strong and compact matrix as reported by the findings of Kaze, et al. [19, 25] and Kamseu, et al. [7]. Hence in these matrices with lower value of  $\text{Si}/\text{Al}$  and  $\text{Si}/\text{Fe}$  ratios, the released Fe, Si and Al species in alkaline medium are not enough to form strong chemical bonds like polysialate (N-A-S-H), ferrosialate (N-A-F-S-H) and ferrisilicate (N-S-F-H) responsible for the development of dense structures that could ensure the better strength. This trend quite matches with the porosity and water absorption values observed in Figures 8 and 9. The geopolymer samples without rice husk ash developed more porosity allowing the retention of water compared to those containing rice husk ash at different dosages which reduces the open voids rendering the matrix more compact and denser. The poor matrices developed by the geopolymer composites without rice husk ash (Figure 11a) are consistent with the XRD and FTIR which revealed that after the reaction, crystalline phases such as kaolinite and goethite initially present in the raw laterite were also found in the XRD of geopolymer products justifying their partial alteration

in alkaline medium. Moreover, the micrographs also show the presence of sheet shapes that might be related to none reacted kaolinite or illite from laterite and sand used as aggregates, respectively. In comparison with mechanical results, it is obvious that the more pronounced microcracks, the lower flexural strengths are recorded (i.e. 13.9, 20.5, 25.01, and 28.81 MPa respectively for geopolymers containing 0; 15 and 25% rice husk ash). When 15 and 25 wt.% of reactive silica is added, it is observed the reduction of open voids and microcracks compared to that of  $GL_{0.5}R_0F_{0.5}S$ -OTC (used as reference without rice husk ash).

The ESEM micrographs of the STC-cured geopolymer composites are shown in Figure 12. In comparison with those of OTC, it can be observed that the structures are denser and homogeneous. This is due to the fact that the presence of water in form of humidity in the system during the reaction is controlled and participates to the reaction, making iron more able to form strong polymers (ferrisilicates). This compactness of structure is linked to the reaction between Si and Fe compounds resulting in formation of covalent Fe-Si bonds. The micrographs also revealed that as the amount of rice husk ash increases, the structure became denser; as observed in OTC curing as shown in Figures 11a-c. The bending strength values increased as the microcracks decreased, justifying the high strengths achieved on samples when applying steam curing (22.30, 24.92, and 56.41 MPa respectively for the geopolymer products having 15 and 25% of rice husk ash). Thus, adding rice husk ash in the whole system provided more Si-oligomers in contact of alkaline solution when steam chamber curing is applied. This released more Si species favored the polymerization with other constituents like Al and Fe that ensured the strong structure and high mechanical performances (Figure 10). However, it is necessary to note that, applying steam chamber curing cycle under controlled humidity is the main parameter that permitted high strength development and more compacted structure. This is the consequence of the reactions of dissolution and polycondensation under controlled humidity. At high magnification (x1000) the sheets are furthermore represented. At lower scales (x250) the presence of few pores and open voids are not uniformly distributed in the matrices.

The curing mode affects the densification of the geopolymer composites: when the curing mode is OTC (characterized by the quickly departure of water) the structure is less dense compared to STC (controlled moisture). Results in agreement with the mechanical strength which gave higher values for STC with dense structures than OTC (Figure 10). This quite matches with the findings of Kamseu et al. [7] who's demonstrated that using steam curing in

545 the synthesis of geopolymer composites from iron-rich laterite allows the formation of  
 546 ferrosialate and ferrisilicates.

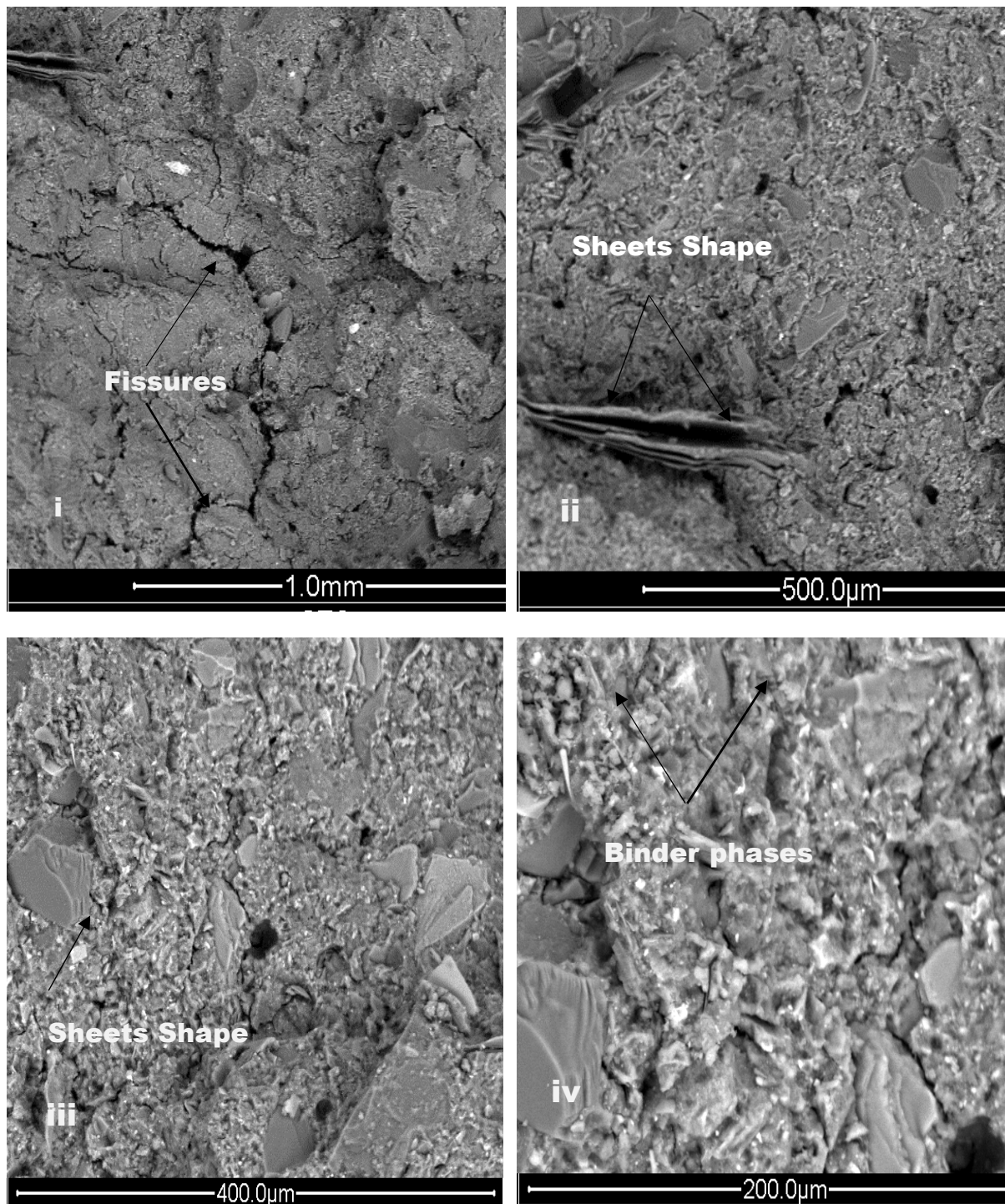


Figure11a: ESEM image of  $GL_{0.5}R_0F_{0.5}S$  geopolymer cured at oven curing temperature (OTC).



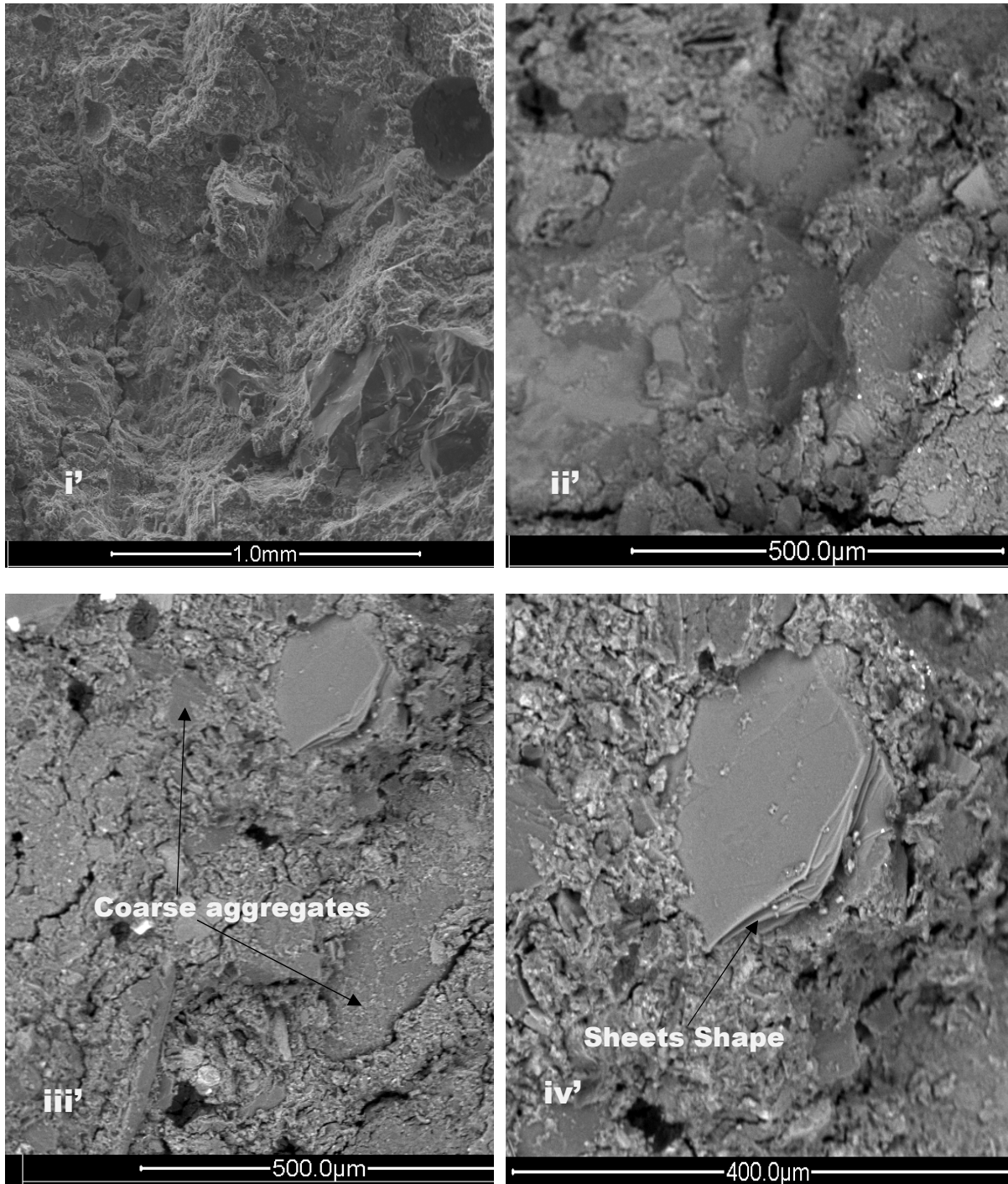
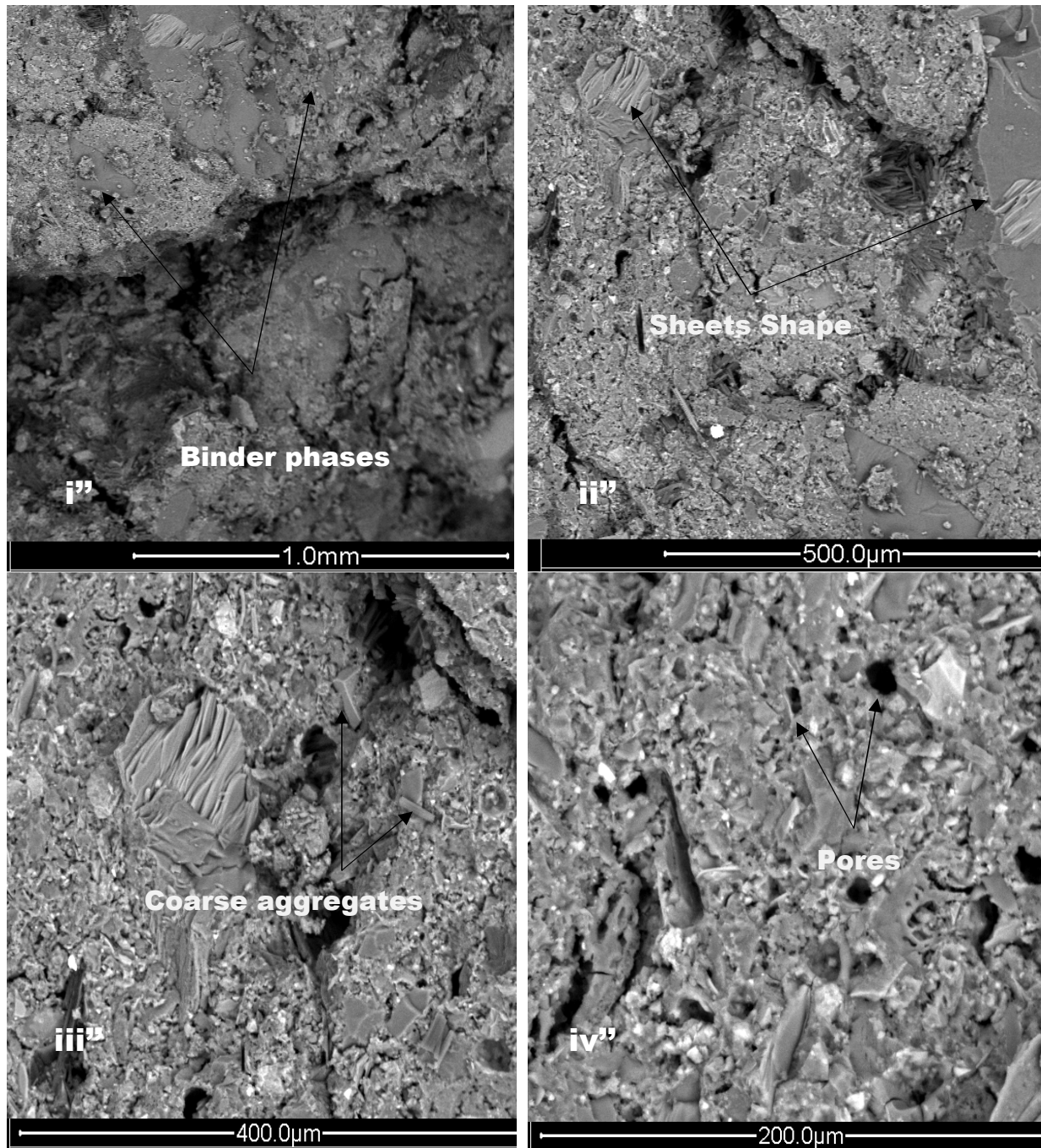


Figure11b: ESEM image of  $GL_{0.35}R_{0.15}F_{0.5}S$  geopolymer cured at oven curing temperature (OTC).



548 Figure11c: ESEM image of  $GL_{0.25}R_{0.25}F_{0.5}S$  geopolymer cured at oven curing temperature  
 549 (OTC).

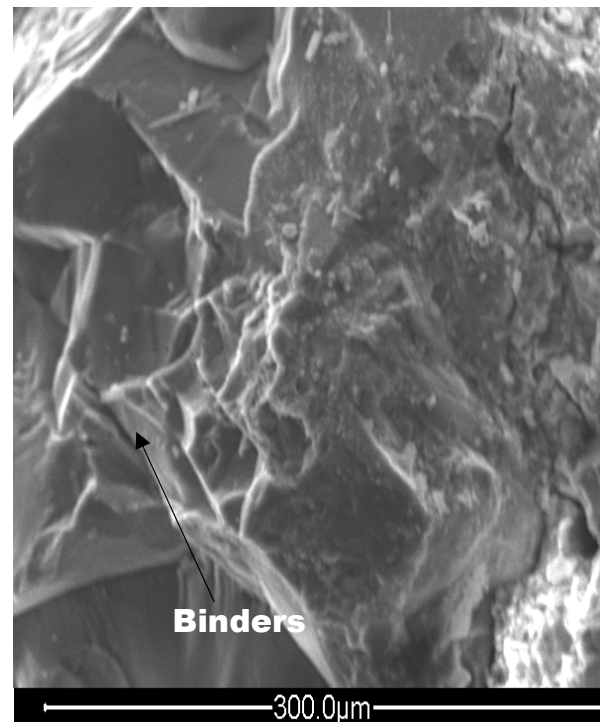
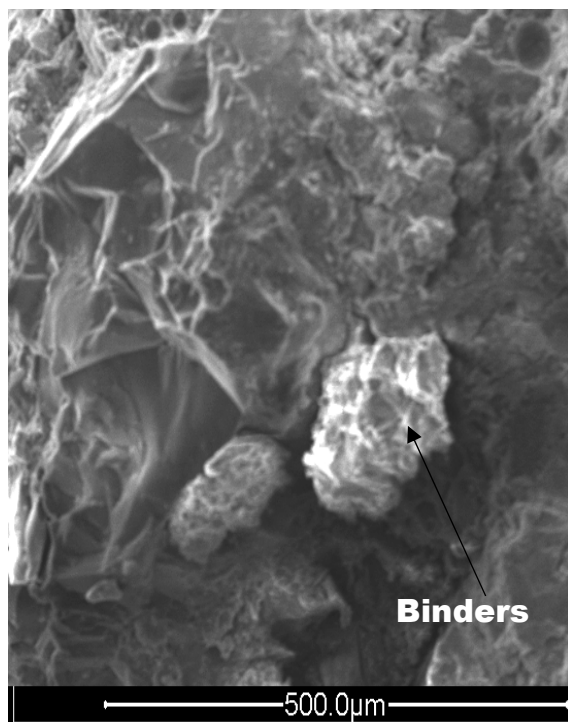
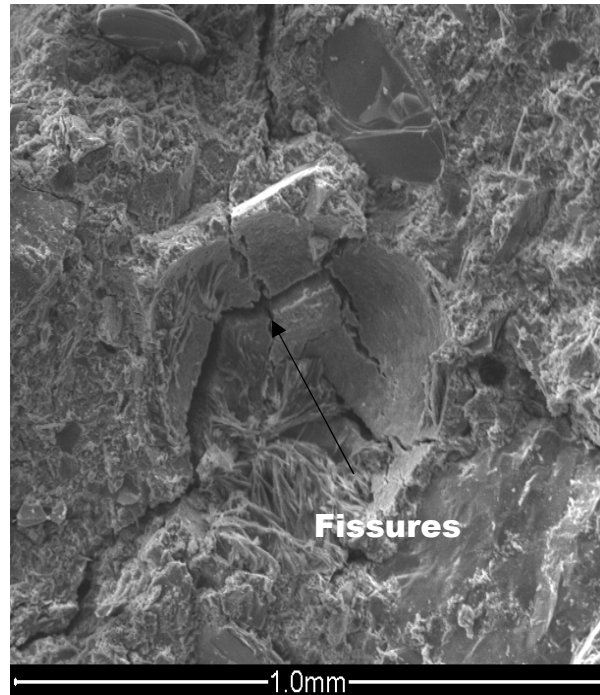
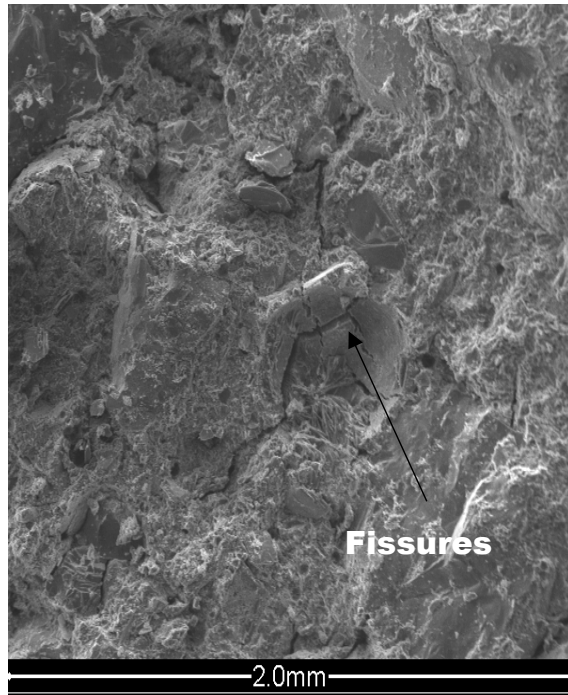
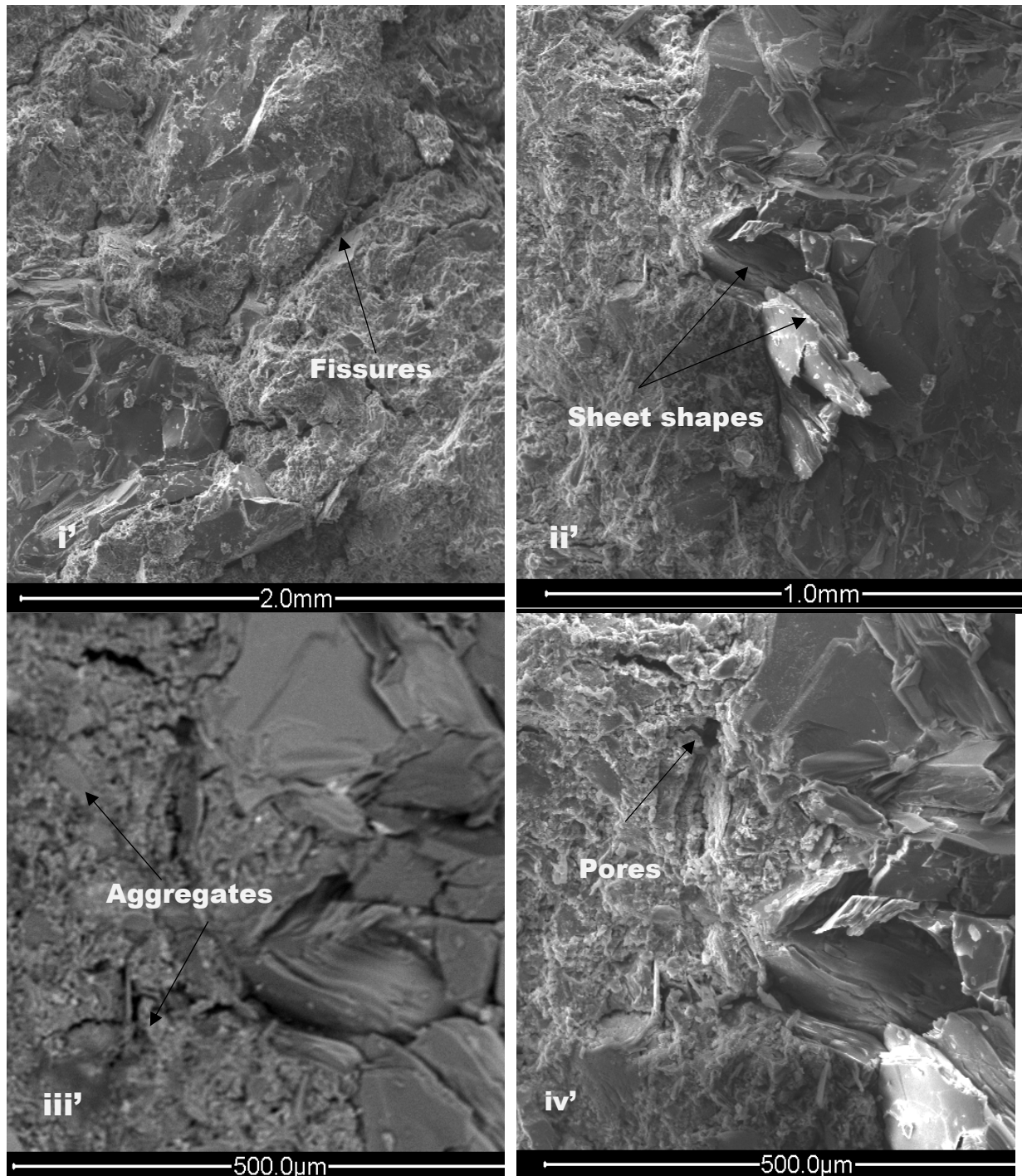


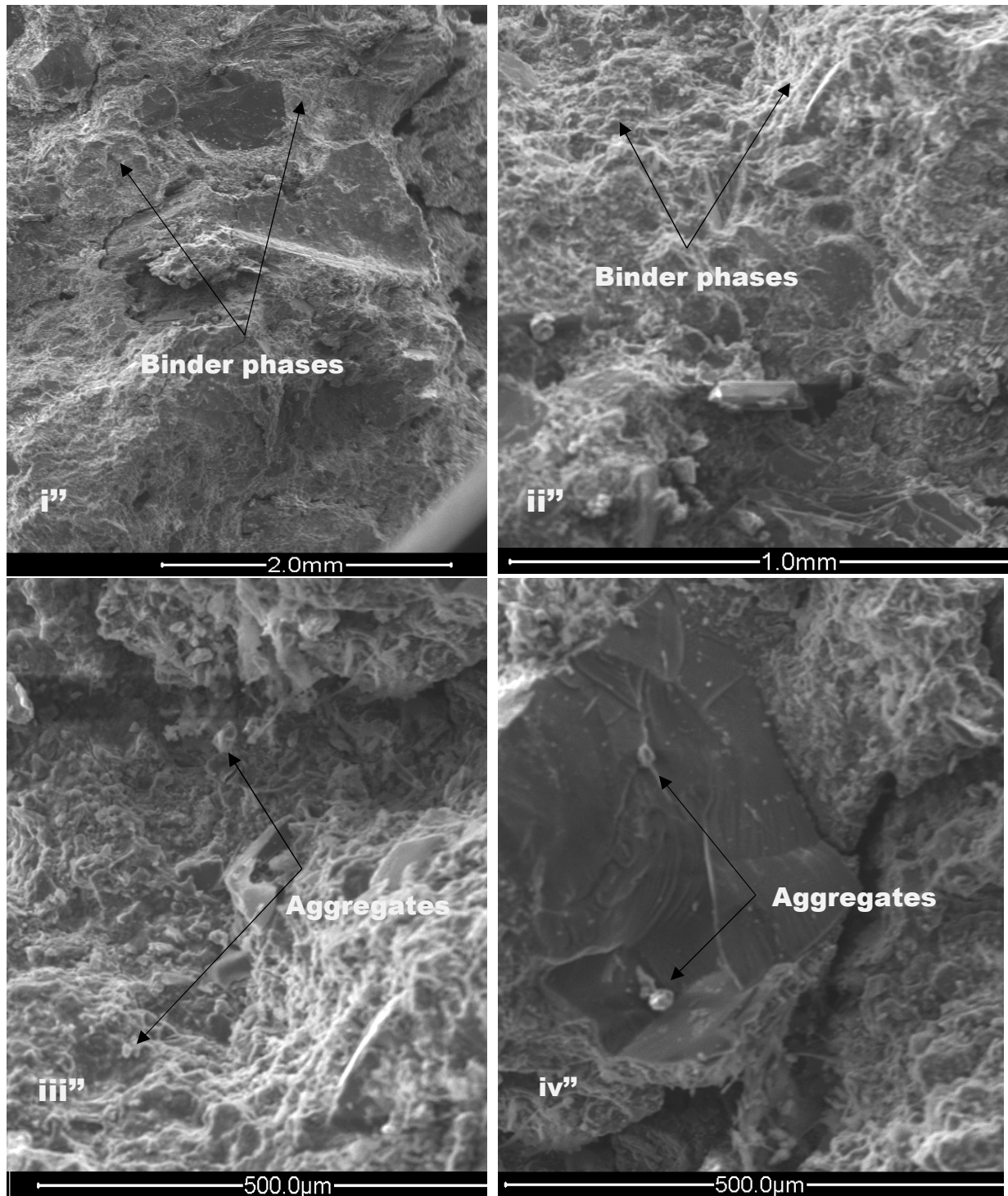
Figure12a: ESEM image of  $GL_{0.5}R_0F_{0.5}S$  geopolymer cured at steam curing temperature (STC).



551 Figure12b: ESEM image of  $GL_{0.35}R_{0.15}F_{0.5}S$  geopolymer cured at steam curing temperature  
 552 (STC).

553 .





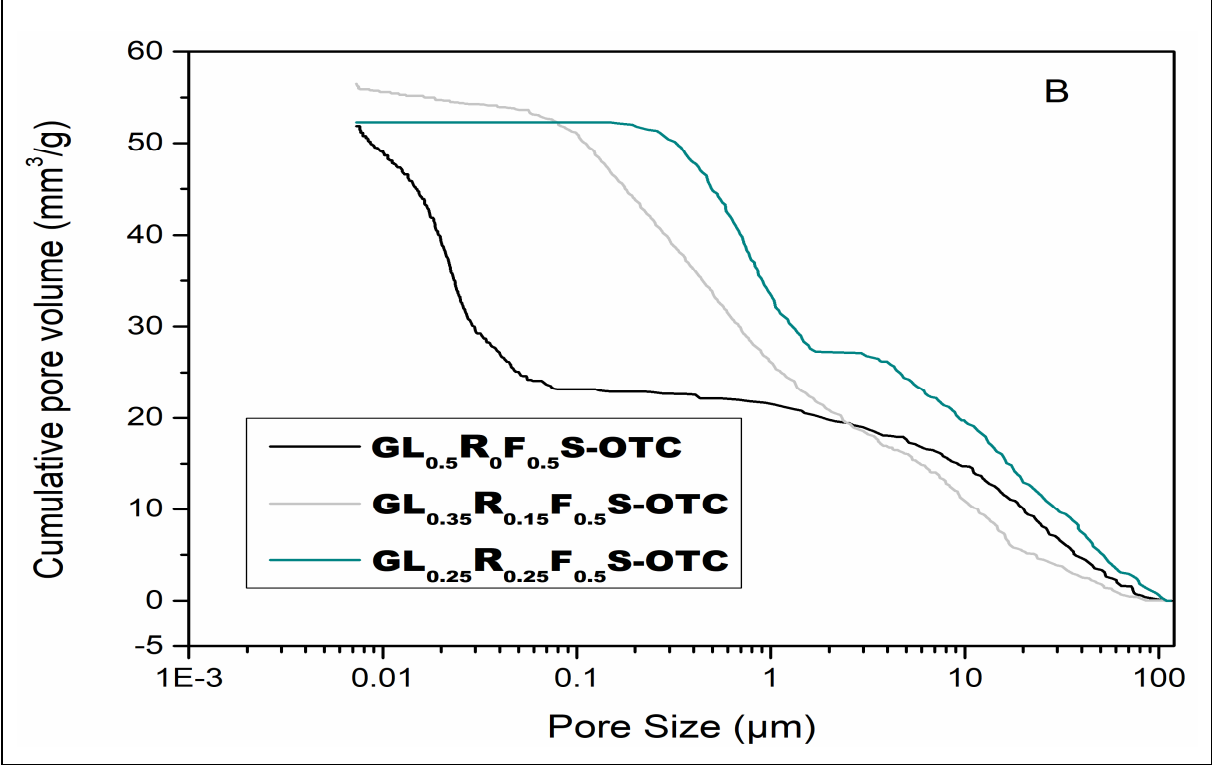
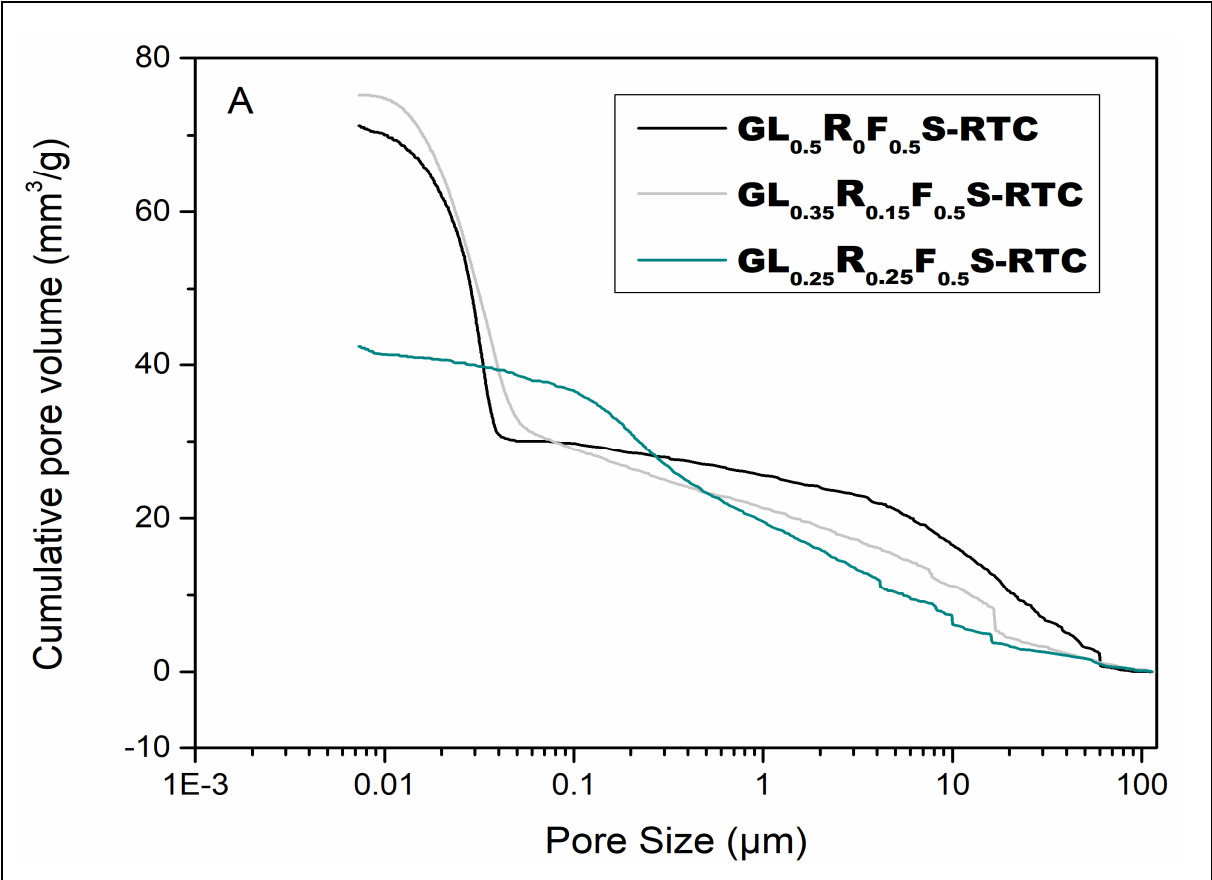
554 Figure12c: ESEM image of  $GL_{0.25}R_{0.25}F_{0.5}S$  geopolymer cured at steam curing temperature  
 555 (STC).

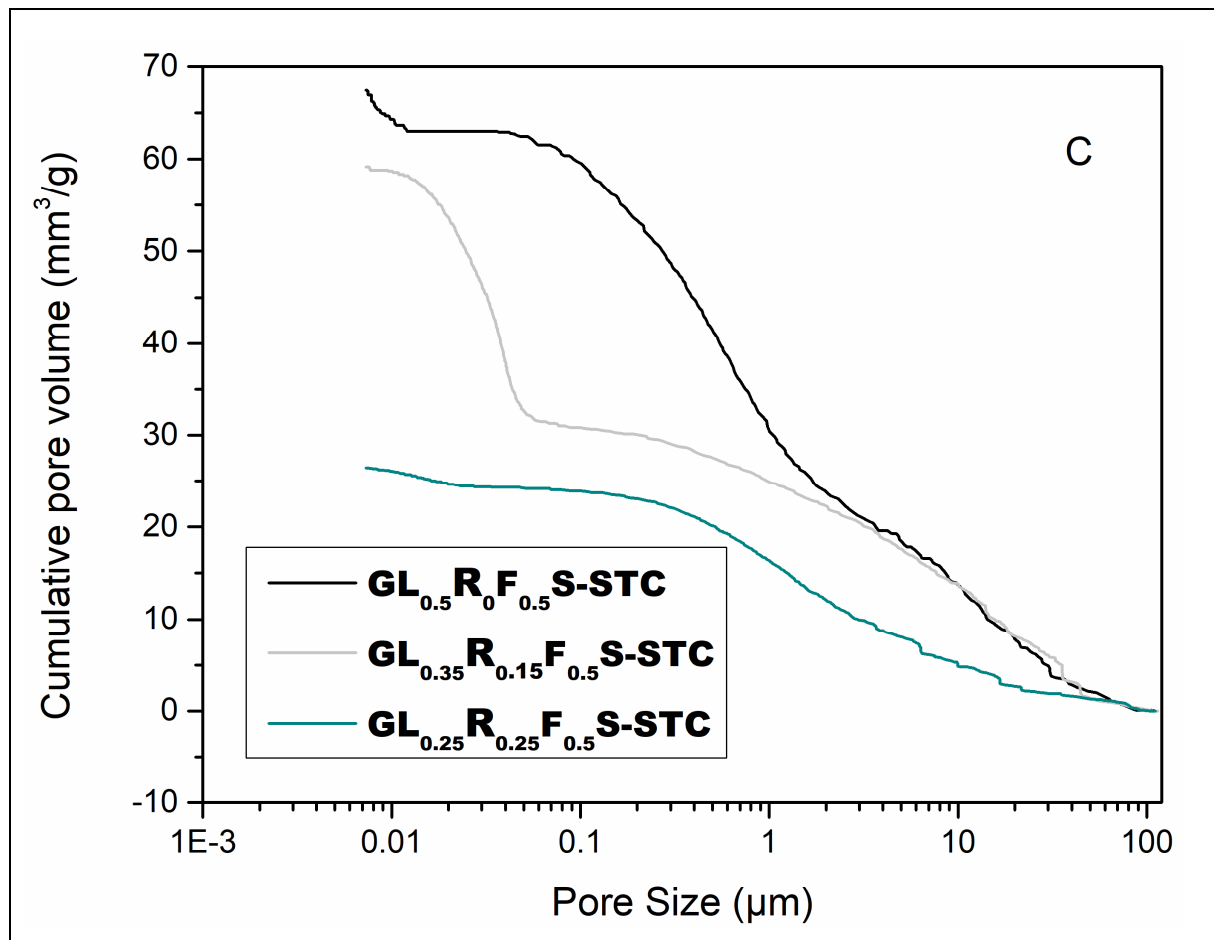
### 556 3.2.5 Mercury intrusion porosimetry (MIP)

557 The variation of cumulative pore volume of selected geopolymer composites namely  
 558  $GL_{0.5}R_0F_{0.5}S$ ,  $GL_{0.35}R_{0.15}F_{0.5}S$ , and  $GL_{0.25}R_{0.25}F_{0.5}S$ , are presented in Figure 13. It is observed

that curing cycles significantly affect the cumulative pore volume recorded in all the geopolymer composites. For the geopolymer composites  $GL_{0.5}R_0F_{0.5}S$ ,  $GL_{0.35}R_{0.15}F_{0.5}S$ , and  $GL_{0.25}R_{0.25}F_{0.5}S$ , the values of cumulative pore volume are 71.30, 75.24, and 42.41 mm<sup>3</sup>/g, respectively, when applied the room temperature curing (RTC). This reduction is linked to the soluble action of Si species from rice husk ash that reacts with Al and Fe species then fills the pore spaces.

In case of the following use of oven curing (OTC) and steam curing (STC) cycles, these values are 51.90, 56.53, and 52.30 mm<sup>3</sup>/g; 67.50, 59.20, and 26.44 mm<sup>3</sup>/g, respectively, for  $GL_{0.5}R_0F_{0.5}S$ ,  $GL_{0.35}R_{0.15}F_{0.5}S$ , and  $GL_{0.25}R_{0.25}F_{0.5}S$  geopolymer specimens. The reduction in specific pore volume with the incorporation of rice husk ash as well as the use of OTC and STC curing modes is linked to the densification of structure resulting in few accessible pores within the matrices. In addition, this reduction more pronounced in sample  $GL_{0.25}R_{0.25}F_{0.5}S$  containing 25 wt% of rice husk ash, could be explained by the fact applying the STC mode under controlled humidity optimized the geopolymerization reaction. This is followed by the good polycondensation and polymerization between Si, Al and Fe species rendering the matrix more homogeneous with few available open voids, micro-voids and capillary pores. Hence adding rice husk ash positively improves the reactivity of laterite based geopolymer composites when applying a steam curing at 80 °C under controlled humidity (65%) leading to the formation of iron silicate compounds which contributed in reinforcement of the structures. The high values of specific pore volume recorded on  $GL_{0.5}R_0F_{0.5}S$  sample (51.90, 67.50 and 71.30 mm<sup>3</sup>/g; when applying OTC, STC and RTC curing modes, respectively) without rice husk ash quite matches with its microstructure which exhibited some open voids and micro-fissures compared to others. This is likely due to the poor cohesion between different components caused by the low Si/Al ratio in corroded laterite from the alteration of kaolinite by iron minerals as reported by others [7]. Therefore, the combined action of fine aggregates and rice husk ash filled the voids and established the good bonding strength or cross-linking between different constituents with less pores in the laterite based geopolymer composite matrices when applied OTC and STC curing modes than RTC (Figures 13b and 13c). Similar trend was noticed by others who replaced metakaolin with fine aggregates (granite, sand, pegmatite, feldspar, etc.) and found that the geopolymer matrix became denser and compact with lower porosity [29, 45, 46].



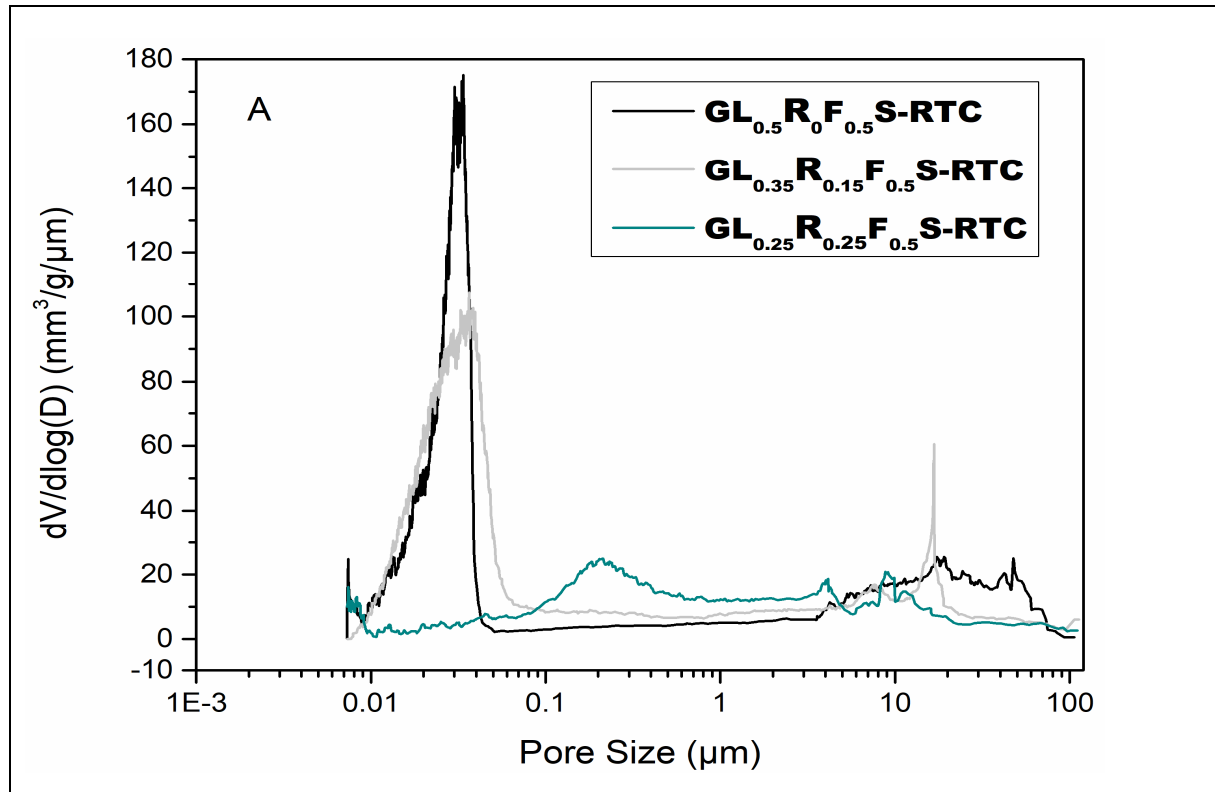


594 Figure 13. Cumulative pore volume distribution of laterite based geopolymer composites  
 595 applied RTC (A), OTC (B), and STC (C) curing cycles.

596 Figure 14 displays the pore size distribution within the microstructure of selected  
 597  $GL_{0.5}R_0F_{0.5}S$ ,  $GL_{0.35}R_{0.15}F_{0.5}S$ , and  $GL_{0.25}R_{0.25}F_{0.5}S$ , geopolymer composites, respectively  
 598 (Figure 14a, 14b and 14c). From Figure 14, it observed that in the samples  $GL_{0.5}R_0F_{0.5}S$  the  
 599 distribution of pores is bimodal and ranged between 0.01-0.1  $\mu m$  and 5-100  $\mu m$ , 0.01-0.1  $\mu m$   
 600 and 1-100  $\mu m$ , when applied RTC and OTC curing modes. Except in STC curing mode where  
 601 it is noticed a trimodal pore size distribution ranged at 0.009-0.0015  $\mu m$ , 0.1-7.0  $\mu m$  and 8.0-  
 602 100  $\mu m$ . The incorporation of reactive silica (contained in rice husk ash) into laterite based  
 603 geopolymer composites shifted the pores band towards lower values (Figure 14). Thus, using  
 604 reactive silica and fine aggregates contributes to reduce the macropores either by parking  
 605 particles effect or establishment of Si-O-Fe and Si-O-Al leading to formation of ferrisilicate  
 606 that densifies the matrix. However, the last interval of pore size distribution in all the  
 607 geopolymer samples is likely due to presence of open voids and microfissures that could not



608 be taken into account from MIP measurements. According to Kamseu, et al. [7] and Kaze, et  
609 al. [25] these large voids or pores are either attributed to the air bubbles released from the  
610 corrosion of iron minerals in alkaline activator or sudden evaporation of water molecules  
611 when applying oven curing without controlled humidity.



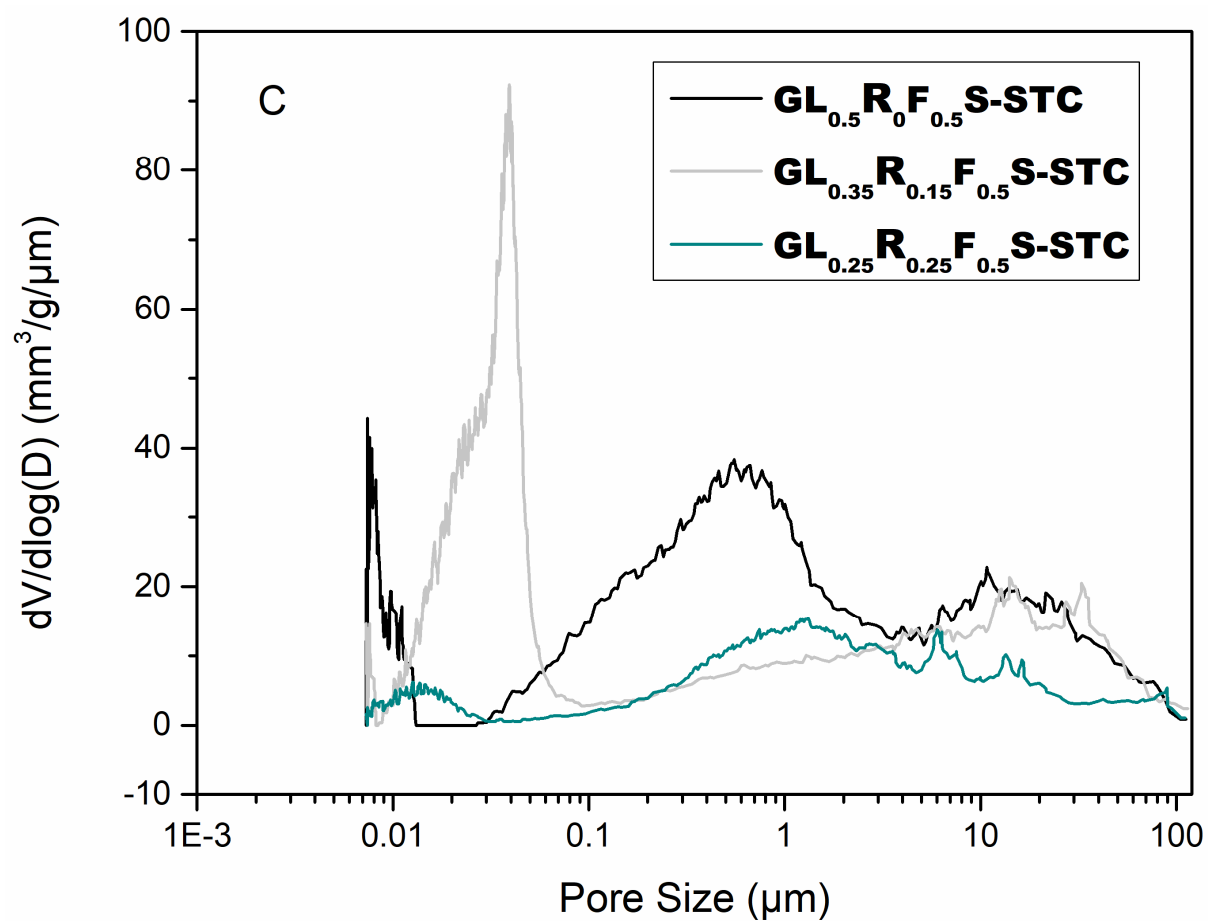
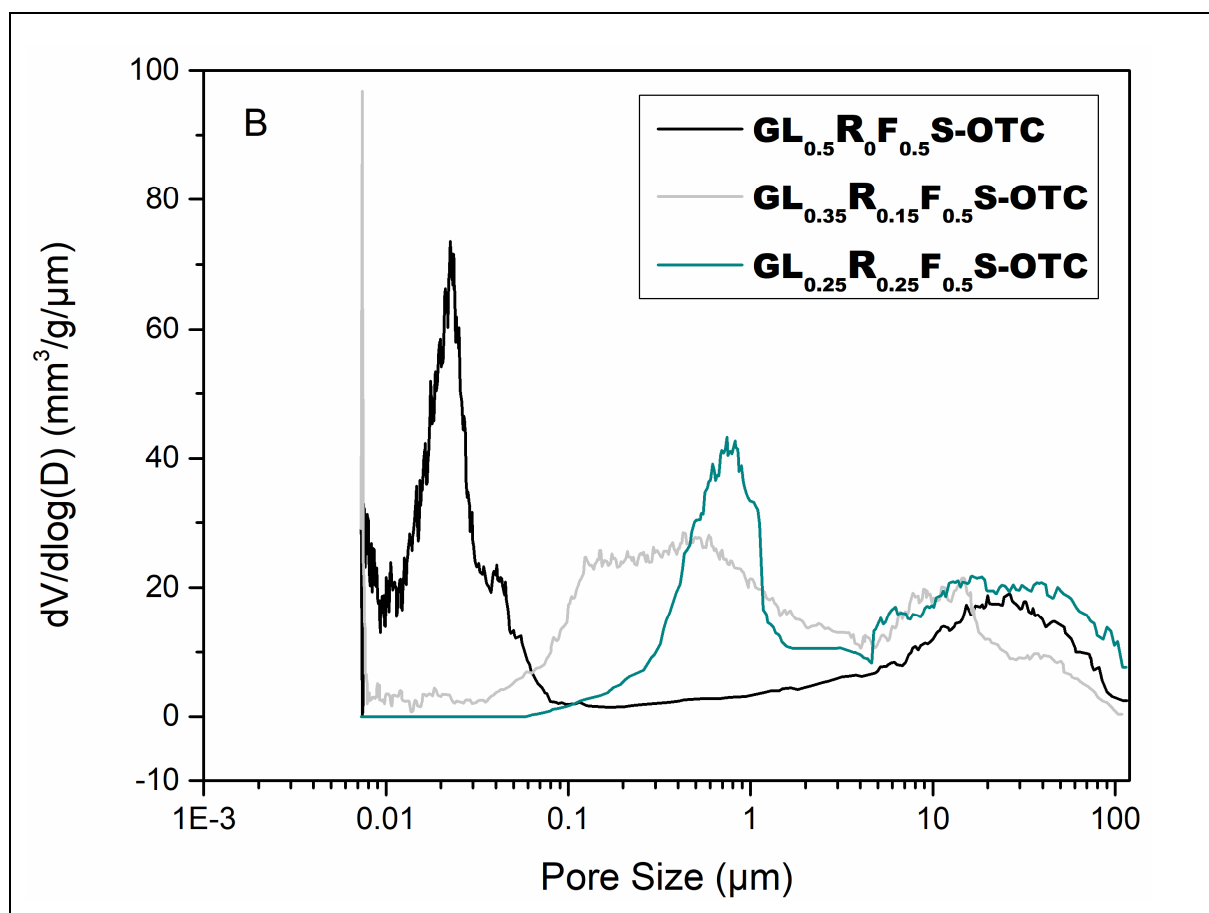
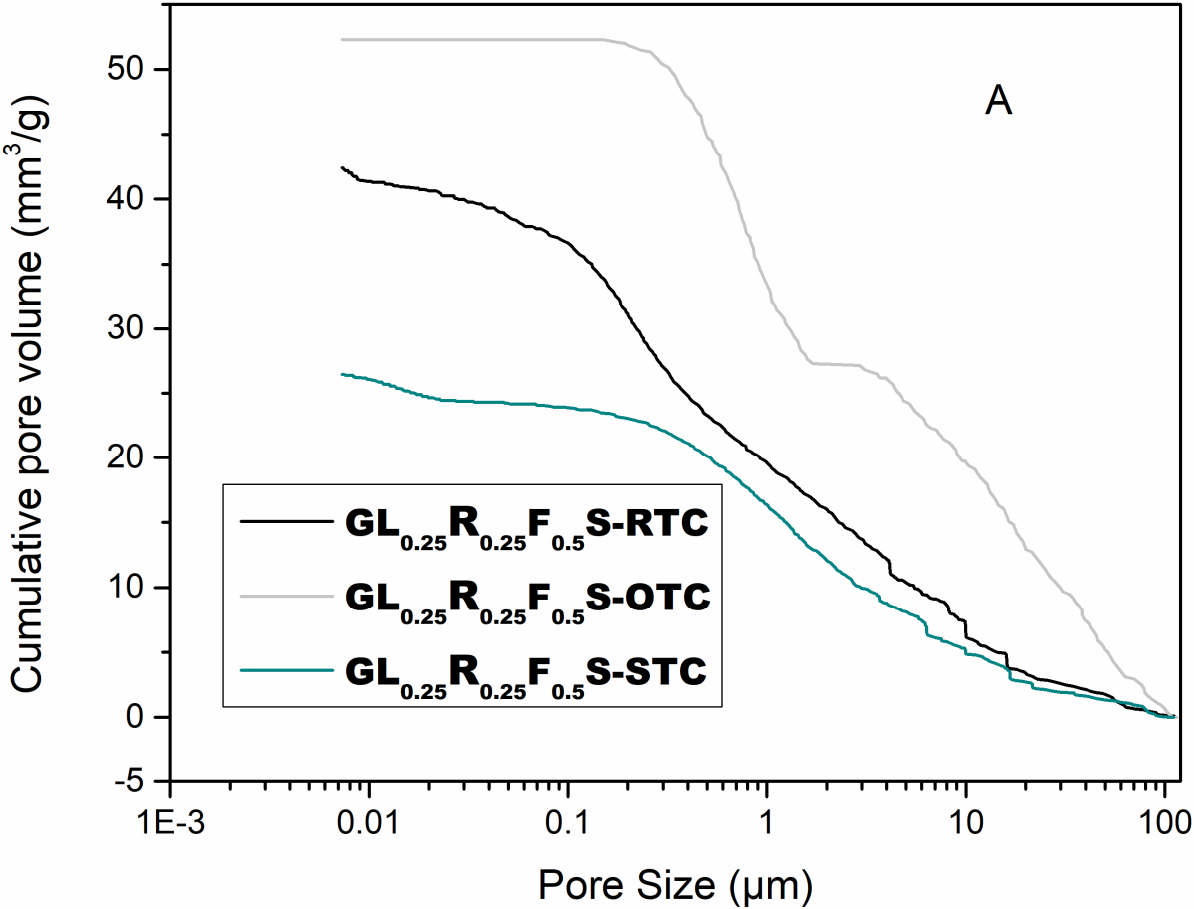


Figure 14. Pore size distribution of laterite based geopolymer composites applied RTC (A), OTC (B), and STC (C) curing cycles.

Figure 15 highlights the superimposed variations of specific pore volume (Figure 15a) and pore size distribution (Figure 15b) of the selected formulation  $GL_{0.25}R_{0.25}F_{0.5}S$  (geopolymer composite which ensured high strength) at different applied curing cycles. From Figure 15a, the specific volume is  $42.41 \text{ mm}^3/\text{g}$  when applied RTC mode, this value increases up to  $52.30 \text{ mm}^3/\text{g}$  in OTC mode. This increase when applied the oven curing cycle (OTC) mode is due to the accessible voids and pores that are formed within the geopolymer matrix. It is well known in the literature that increase the curing temperature yields better cohesion, densification and strength development of the end geopolymer products [9, 47, 48]. In the case studied, using an oven curing mode (OTC) at  $80^\circ\text{C}$ , favors at the same time the dissolution of raw materials and the sudden departure of water molecules leading to the formation of open voids observed on the micrographs. This is related due to none equilibrium between the different constituents to form a stable matrix compared to that of fly ash and metakaolin. With this curing mode (OTC) even the end products were dense and strong but they exhibited porous matrix with sponge-like structure [7]. Similar structure has been observed in the finding of Kaze, et al. [25] and Kamseu, et al. [7] when combined laterite with reactive silica at different dosages followed by the oven curing at  $90^\circ\text{C}$  without controlled humidity. When the steam curing cycle (STC) under controlled humidity ( $80^\circ\text{C}$ , 65%) is used, the specific pore volume decreases and reaches  $26.44 \text{ mm}^3/\text{g}$ . hence in the steam curing mode (STC) increasing the curing temperature ( $80^\circ\text{C}$ ) accompanied with controlled humidity optimized the geopolymerization process that helped to form rigid and homogeneous matrix with the gel interconnected pores. This curing mode allows a process that produces the laterite geopolymer composites with dense structures that could resist in extreme conditions compared to the porous matrices of Kaze, et al. [25] and Kamseu, et al. [7]. This is well explained in Figure 15b, in which the STC exhibits lower porosity followed by OTC and RTC, respectively. This result is in agreement with SEM analysis and mechanical properties. Thus, applying the steam curing mode in the synthesis of laterite based geopolymer composites is the best way for the development of performant and sustainable materials.

642



643

644

645

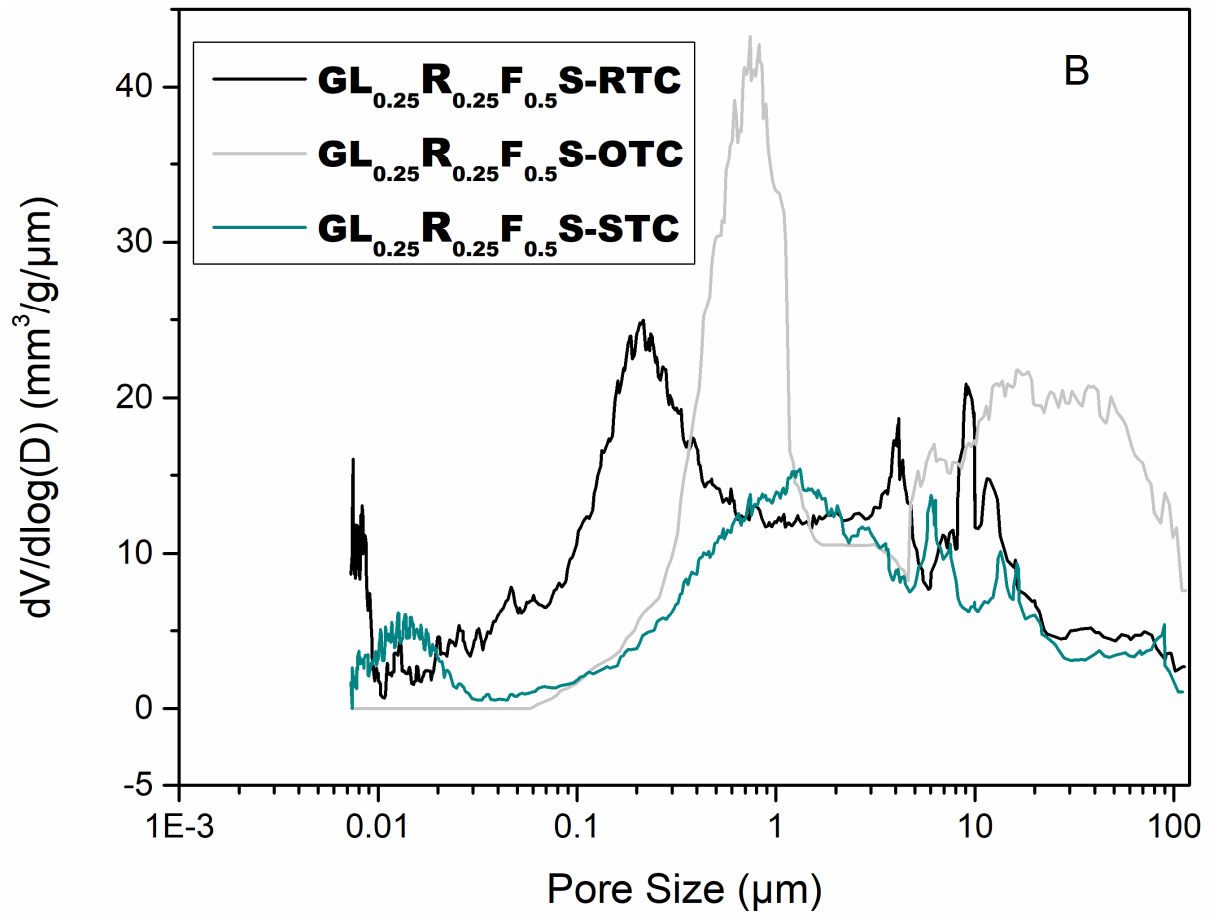


Figure 15. Cumulative pore volume (A) and pore size distribution (B) of laterite based geopolymer composite  $\text{GL}_{0.25}\text{R}_{0.25}\text{F}_{0.5}\text{S}$  sample applying RTC (A), OTC (B), and STC (C) curing cycles.

#### 4. Conclusion

This work deals with the elaboration and characterization of laterite based geopolymer composites applying the different curing cycles as follows; room curing temperature (RTC), oven curing temperature (OTC) and steam chamber curing temperature (STC) with controlled humidity. The main objective of this work is to identify the most appropriate curing cycle for the achievement of high strength matrices with reduced porosity. After investigation the following conclusions can be drawn.

- Room Temperature curing (RTC) does not allow the efficient participation of reactive iron ions present in goethite, hematite and others oxyhydrates.
- Oven Curing (OTC) successfully activates iron ions; however, the earlier evaporation of water affects the complete dissolution and the hinder, the efficiency of the polycondensation of the final matrices.
- Applying the steam curing (STC) under controlled humidity ( $> 65\%$ ) optimized the geopolymerization reaction, improved the polymerization/polycondensation, reduced the porosity within the matrices resulting in high mechanical strength;

- The low flexural strength recorded on the samples applying OTC and RTC curing cycles is linked to the none controlled of the release water during the drying step that led the formation of cracks, fissures and open voids within the matrices that weakened the characteristic performances;
- Adding the reactive silica in the whole system allowed the newly formed phase like iron silicate compounds (according to XRD analysis) next to amorphous sodium polysialate, polyferrosialate and ferrisilicate binders that extend the geopolymer network and contribute to the densification of matrix; it also promoted the more release of Si-oligomers that polymerize with other constituents (Al- and Fe- species) and make the matrix stronger and compact;

The end products obtained in the present study are sustainable, green and could be found application in buildings and construction, particularly where high performances are required.

## 5 Acknowledgments

This project received the contribution of the FLAIR fellowship African Academic of Science and the Royal Society through the funding N° FLR/R1/201402. The authors are also grateful Ingessil S.r.l., Verona, Italy, for providing sodium silicate used. JNNF is acknowledging the financial support from AUF (Agence Universitaire de la Francophonie) through the funding N° 0950740/DRACGL2018 for her stay in IRCER, UMRCNRS 7315, Limoges France.

## 6 References

1. Bewa, C.N., H.K. Tchakouté, C.H. Rüschler, E. Kamseu, and C. Leonelli, *Influence of the curing temperature on the properties of poly (phospho-ferro-siloxo) networks from laterite*. Journal SN Applied Sciences, 2019. **1**(8): p. 916.
2. Kaze, C.R., J.N.Y. Djobo, A. Nana, H.K. Tchakoute, E. Kamseu, U.C. Melo, C. Leonelli, and H. Rahier, *Effect of silicate modulus on the setting, mechanical strength and microstructure of iron-rich aluminosilicate (laterite) based-geopolymer cured at room temperature*. Journal of Ceramics International, 2018. **44**(17): p. 21442-21450.
3. Boum, R.B.E., C.R. Kaze, J.G.D. Nemaleu, V.B. Djaoyang, N.Y. Rachel, P.L. Ninla, F.M. Owono, and E. Kamseu, *Thermal behaviour of metakaolin–bauxite blends geopolymer: microstructure and mechanical properties*. SN Applied Sciences, 2020. **2**(8): p. 1358.
4. Davidovits, J., *Geopolymers: inorganic polymeric new materials*. Journal of Thermal Analysis calorimetry, 1991. **37**(8): p. 1633-1656.
5. Nobouassia Bewa, C., H.K. Tchakouté, D. Fotio, C.H. Rüschler, E. Kamseu, and C. Leonelli, *Water resistance and thermal behavior of metakaolin-phosphate-based geopolymer cements*. Journal of Asian Ceramic Societies, 2018. **6**(3): p. 271-283.
6. Davidovits, J. and R. Davidovits, *Ferro-sialate Geopolymers (-Fe-O-Si-O-Al-O-)*. 2020.
7. Kamseu, E., C.R. Kaze, J.N.N. Fekoua, U.C. Melo, S. Rossignol, and C. Leonelli, *Ferrisilicates formation during the geopolymerization of natural Fe-rich aluminosilicate precursors*. Materials Chemistry and Physics, 2020. **240**: p. 122062.
8. Tchakouté, H.K., S.J. Melele, A.T. Djamien, C.R. Kaze, E. Kamseu, C.N. Nansu, C. Leonelli, and C.H. Rüschler, *Microstructural and mechanical properties of poly (sialate-siloxo) networks*

obtained using metakaolins from kaolin and halloysite as aluminosilicate sources: A comparative study. *Journal Applied Clay Science*, 2020. **186**: p. 105448.

9. Kaze, C.R., G.L. Lecomte-Nana, E. Kamseu, P.S. Camacho, A.S. Yorkshire, J.L. Provis, M. Duttine, A. Wattiaux, and U.C. Melo, *Mechanical and physical properties of inorganic polymer cement made of iron-rich laterite and lateritic clay: A comparative study*. *Cement and Concrete Research*, 2021. **140**: p. 106320.

10. Kamseu, E., A. Rizzuti, C. Leonelli, and D. Perera, *Enhanced thermal stability in K<sub>2</sub>O-metakaolin-based geopolymer concretes by Al<sub>2</sub>O<sub>3</sub> and SiO<sub>2</sub> fillers addition*. *Journal of Materials Science* 2010. **45**(7): p. 1715-1724.

11. Tchakouté, H.K., C.H. Rüschler, E. Kamseu, F. Andreola, and C. Leonelli, *Influence of the molar concentration of phosphoric acid solution on the properties of metakaolin-phosphate-based geopolymer cements*. *Applied Clay Science*, 2017. **147**: p. 184-194.

12. Zhang, Z., H. Wang, X. Yao, and Y. Zhu, *Effects of halloysite in kaolin on the formation and properties of geopolymers*. *Cement and Concrete Composites*, 2012. **34**(5): p. 709-715.

13. Zivica, V., M.T. Palou, and T.I.L. Bágel, *High strength metahalloysite based geopolymer*. *Journal Composites Part B: Engineering* 2014. **57**: p. 155-165.

14. Assaedi, H., T. Alomayri, C.R. Kaze, B.B. Jindal, S. Subaer, F. Shaikh, and S. Alraddadi, *Characterization and properties of geopolymer nanocomposites with different contents of nano-CaCO<sub>3</sub>*. *Construction and Building Materials*, 2020. **252**: p. 119137.

15. Mustakim, S.M., S.K. Das, J. Mishra, A. Aftab, T.S. Alomayri, H.S. Assaedi, and C.R. Kaze, *Improvement in Fresh, Mechanical and Microstructural Properties of Fly Ash- Blast Furnace Slag Based Geopolymer Concrete By Addition of Nano and Micro Silica*. *Silicon*, 2020.

16. Walling, S.A., S.A. Bernal, L.J. Gardner, H. Kinoshita, and J.L.J.R.a. Provis, *Blast furnace slag-Mg (OH)<sub>2</sub> cements activated by sodium carbonate*. 2018. **8**(41): p. 23101-23118.

17. Djobo, J.N.Y., A. Elimbi, H.K. Tchakouté, and S. Kumar, *Mechanical activation of volcanic ash for geopolymer synthesis: effect on reaction kinetics, gel characteristics, physical and mechanical properties*. *Journal RSC advances*, 2016. **6**(45): p. 39106-39117.

18. Lemougna, P.N., U.C. Melo, M.-P. Delplancke, and H. Rahier, *Influence of the activating solution composition on the stability and thermo-mechanical properties of inorganic polymers (geopolymers) from volcanic ash*. *Journal Construction Building Materials* 2013. **48**: p. 278-286.

19. Kaze, R., L.B. à Mougna, M.F. Djouka, A. Nana, E. Kamseu, U.C. Melo, and C. Leonelli, *The corrosion of kaolinite by iron minerals and the effects on geopolymerization*. *Journal of Applied Clay Science*, 2017. **138**: p. 48-62.

20. Lecomte-Nana, G., H. Goure-Doubi, A. Smith, A. Wattiaux, and G. Lecomte, *Effect of iron phase on the strengthening of lateritic-based "geomimetic" materials*. *Journal of Applied clay science*, 2012. **70**: p. 14-21.

21. Lemougna, P.N., K.-t. Wang, Q. Tang, E. Kamseu, N. Billong, U.C. Melo, and X.-m. Cui, *Effect of slag and calcium carbonate addition on the development of geopolymer from indurated laterite*. *Journal of Applied Clay Science*, 2017. **148**: p. 109-117.

22. Lemougna, P.N., A.B. Madi, E. Kamseu, U.C. Melo, M.-P. Delplancke, and H. Rahier, *Influence of the processing temperature on the compressive strength of Na activated lateritic soil for building applications*. *Journal Construction Building Materials* 2014. **65**: p. 60-66.

23. Nkwaju, R., J. Djobo, J. Nouping, P. Huisken, J. Deutou, and L. Courard, *Iron-rich laterite-bagasse fibers based geopolymer composite: Mechanical, durability and insulating properties*. Journal Applied Clay Science, 2019. **183**: p. 105333.
24. Poudeu, R.C., C.J. Ekani, C.N. Djangang, and P. Blanchart, *Role of Heat-Treated Laterite on the Strengthening of Geopolymer Designed with Laterite as Solid Precursor Role of Heat-Treated Laterite on the Strengthening of Geopolymer Designed with Laterite as Solid Precursor*. Annales de Chimie - Science des Matériaux, 2020. **43**(6): p. 359-367.
25. Kaze, R.C., L.M. Beleuk à Mounkam, M. Cannio, R. Rosa, E. Kamseu, U.C. Melo, and C. Leonelli, *Microstructure and engineering properties of Fe<sub>2</sub>O<sub>3</sub> (FeO)-Al<sub>2</sub>O<sub>3</sub>-SiO<sub>2</sub> based geopolymer composites*. Journal of Cleaner Production, 2018. **199**: p. 849-859.
26. Gualtieri, M.L., M. Romagnoli, S. Pollastri, and A.F. Gualtieri, *Inorganic polymers from laterite using activation with phosphoric acid and alkaline sodium silicate solution: mechanical and microstructural properties*. Journal of Cement Concrete Research **2015**. **67**: p. 259-270.
27. Gomes, K.C., G.S. Lima, S.M. Torres, S.R. de Barros, I.F. Vasconcelos, and N.P. Barbosa. *Iron distribution in geopolymer with ferromagnetic rich precursor*. in *Materials Science Forum*. 2010. Trans Tech Publ.
28. Nana, A., J. Ngouné, R.C. Kaze, L. Boubakar, S.K. Tchounang, H.K. Tchakouté, E. Kamseu, and C. Leonelli, *Room-temperature alkaline activation of feldspathic solid solutions: Development of high strength geopolymers*. Journal Construction Building Materials **2019**. **195**: p. 258-268.
29. Kamseu, E., M. Cannio, E.A. Obonyo, F. Tobias, M.C. Bignozzi, V.M. Sglavo, and C. Leonelli, *Metakaolin-based inorganic polymer composite: Effects of fine aggregate composition and structure on porosity evolution, microstructure and mechanical properties*. Cement and Concrete Composites, 2014. **53**: p. 258-269.
30. Tchadjié, L.N., J.N.Y. Djobo, N. Ranjbar, H.K. Tchakouté, B.B.D. Kenne, A. Elimbi, and D. Njopwouo, *Potential of using granite waste as raw material for geopolymer synthesis*. Ceramics International, 2016. **42**(2, Part B): p. 3046-3055.
31. Vijayalakshmi, M., A.S.S. Sekar, and G. Ganesh prabhu, *Strength and durability properties of concrete made with granite industry waste*. Construction and Building Materials, 2013. **46**: p. 1-7.
32. ASTM, C.J.C., *Standard test method for density, absorption, and voids in hardened concrete*. 2013.
33. Gallup, D.L., *Iron silicate scale formation and inhibition at the salton sea geothermal field*. Geothermics, 1989. **18**(1): p. 97-103.
34. Gallup, D. and W.J.G. Reiff, *Characterization of geothermal scale deposits by Fe-57 Mössbauer spectroscopy and complementary X-ray diffraction and infra-red studies*. 1991. **20**(4): p. 207-224.
35. Mimboe, A.G., M.T. Abo, J.N.Y. Djobo, S. Tome, R.C. Kaze, and J.G.N. Deutou, *Lateritic soil based-compressed earth bricks stabilized with phosphate binder*. Journal of Building Engineering, 2020. **31**: p. 101465.
36. Kaze, C.R., T. Alomayri, A. Hasan, S. Tome, G.L. Lecomte-Nana, J.G.D. Nemaleu, H.K. Tchakoute, E. Kamseu, U.C. Melo, and H. Rahier, *Reaction kinetics and rheological behaviour of meta-halloysite based geopolymer cured at room temperature: Effect of thermal activation on physicochemical and microstructural properties*. Applied Clay Science, 2020. **196**: p. 105773.
37. Youmoue, M., R.T. Tene Fongang, A. Gharzouni, R.C. Kaze, E. Kamseu, V.M. Sglavo, I. Tonle Kenfack, B. Nait-Ali, and S. Rossignol, *Effect of silica and lignocellulosic additives on the*



- formation and the distribution of meso and macropores in foam metakaolin-based geopolymer filters for dyes and wastewater filtration. *SN Applied Sciences*, 2020. **2**(4): p. 642.
38. Prud'homme, E., A. Autef, N. Essaidi, P. Michaud, B. Samet, E. Joussein, and S. Rossignol, *Defining existence domains in geopolymers through their physicochemical properties*. *Applied Clay Science*, 2013. **73**: p. 26-34.
  39. Essaidi, N., B. Samet, S. Baklouti, and S. Rossignol, *The role of hematite in aluminosilicate gels based on metakaolin*. 2014. **58**(1): p. 1-11.
  40. Nana, A., T.S. Alomayri, P. Venyite, R.C. Kaze, H.S. Assaedi, C.B. Nobouassia, J.V.M. Sontia, J. Ngouné, E. Kamseu, and C. Leonelli, *Mechanical Properties and Microstructure of a Metakaolin-Based Inorganic Polymer Mortar Reinforced with Quartz Sand*. *Silicon*, 2020.
  41. Obonyo, E.A., E. Kamseu, P.N. Lemougna, A.B. Tchamba, U.C. Melo, and C.J.S. Leonelli, *A sustainable approach for the geopolymerization of natural iron-rich aluminosilicate materials*. 2014. **6**(9): p. 5535-5553.
  42. Dimas, D., I. Giannopoulou, and D. Panias, *Polymerization in sodium silicate solutions: a fundamental process in geopolymerization technology*. *Journal of Materials Science*, 2009. **44**(14): p. 3719-3730.
  43. El-Naggar, M.R. and M.I. El-Dessouky, *Re-use of waste glass in improving properties of metakaolin-based geopolymers: Mechanical and microstructure examinations*. *Construction and Building Materials*, 2017. **132**: p. 543-555.
  44. Park, S. and M. Pour-Ghaz, *What is the role of water in the geopolymerization of metakaolin?* *Construction and Building Materials*, 2018. **182**: p. 360-370.
  45. Kamseu, E., C. Ponzoni, C. Tippayasam, R. Taurino, D. Chaysuwan, M.C. Bignozzi, L. Barbieri, and C. Leonelli, *Influence of fine aggregates on the microstructure, porosity and chemico-mechanical stability of inorganic polymer concretes*. *Construction and Building Materials*, 2015. **96**: p. 473-483.
  46. Kamseu, E., C. Ponzoni, C. Tippayasam, R. Taurino, D. Chaysuwan, V.M. Sglavo, P. Thavorniti, and C. Leonelli, *Self-compacting geopolymer concretes: Effects of addition of aluminosilicate-rich fines*. *Journal of Building Engineering*, 2016. **5**: p. 211-221.
  47. Rodrigue Kaze, C., P. Ninla Lemougna, T. Alomayri, H. Assaedi, A. Adesina, S. Kumar Das, G.-L. Lecomte-Nana, E. Kamseu, U. Chinje Melo, and C. Leonelli, *Characterization and performance evaluation of laterite based geopolymer binder cured at different temperatures*. *Construction and Building Materials*, 2020: p. 121443.
  48. Nana, A., R. Cyriaque Kaze, T. Salman Alomayri, H. Suliman Assaedi, J.G. Nemaleu Deutou, J. Ngouné, H. Kouamo Tchakouté, E. Kamseu, and C. Leonelli, *Innovative porous ceramic matrices from inorganic polymer composites (IPCs): Microstructure and mechanical properties*. *Construction and Building Materials*, 2021. **273**: p. 122032.

## Figures and Tables caption